



HAL
open science

New chronological constraints on intense Holocene eruptions and landslide activity at Tacaná volcanic complex (Mexico)

Jesús Alcalá-Reygosa, José Luis Arce, José Luis Macías, Irene Schimmelpfennig, Ricardo Saucedo, Juan Manuel Sánchez, Teodoro Carlón, Rosario Vázquez, Guillermo Cisneros-Máximo, Adrian Jiménez, et al.

► To cite this version:

Jesús Alcalá-Reygosa, José Luis Arce, José Luis Macías, Irene Schimmelpfennig, Ricardo Saucedo, et al.. New chronological constraints on intense Holocene eruptions and landslide activity at Tacaná volcanic complex (Mexico). *Quaternary Geochronology*, 2021, 65, pp.101183. 10.1016/j.quageo.2021.101183 . hal-03226096

HAL Id: hal-03226096

<https://hal.science/hal-03226096>

Submitted on 14 May 2021

HAL is a multi-disciplinary open access archive for the deposit and dissemination of scientific research documents, whether they are published or not. The documents may come from teaching and research institutions in France or abroad, or from public or private research centers.

L'archive ouverte pluridisciplinaire **HAL**, est destinée au dépôt et à la diffusion de documents scientifiques de niveau recherche, publiés ou non, émanant des établissements d'enseignement et de recherche français ou étrangers, des laboratoires publics ou privés.

Journal Pre-proof

New chronological constraints on intense Holocene eruptions and landslide activity at Tacana volcanic complex (Mexico)

Jesús Alcalá-Reygosa, José Luis Arce, José Luis Macías, Irene Schimmelpfennig, Ricardo Saucedo, Juan Manuel Sánchez, Teodoro Carlón, Rosario Vázquez, Guillermo Cisneros-Máximo, Adrian Jiménez, Salvador Fernández, Aster Team

PII: S1871-1014(21)00034-0

DOI: <https://doi.org/10.1016/j.quageo.2021.101183>

Reference: QUAGEO 101183

To appear in: *Quaternary Geochronology*

Received Date: 8 June 2020

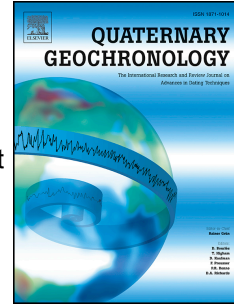
Revised Date: 10 April 2021

Accepted Date: 11 April 2021

Please cite this article as: Alcalá-Reygosa, Jesús., Arce, José.Luis., Macías, José.Luis., Schimmelpfennig, I., Saucedo, R., Sánchez, J.M., Carlón, T., Vázquez, R., Cisneros-Máximo, G., Jiménez, A., Fernández, S., Team, A., New chronological constraints on intense Holocene eruptions and landslide activity at Tacana volcanic complex (Mexico), *Quaternary Geochronology* (2021), doi: <https://doi.org/10.1016/j.quageo.2021.101183>.

This is a PDF file of an article that has undergone enhancements after acceptance, such as the addition of a cover page and metadata, and formatting for readability, but it is not yet the definitive version of record. This version will undergo additional copyediting, typesetting and review before it is published in its final form, but we are providing this version to give early visibility of the article. Please note that, during the production process, errors may be discovered which could affect the content, and all legal disclaimers that apply to the journal pertain.

© 2021 Published by Elsevier B.V.



Abstract

Usual methods are unfortunately unsuitable to accurately date many Holocene deposits and landforms from active Mexican volcanoes. This is notably the case for the Tacaná Volcanic Complex (TVC), located in the State of Chiapas in southern Mexico, and the San Marcos Department in Guatemala. The complex consists of the Chichuj, Tacaná, and San Antonio volcanoes and the Ardillas dome. Tacaná volcano, the main summit of the TVC, collapsed 15 ± 5 ka ago ($^{40}\text{Ar}/^{39}\text{Ar}$), producing the Agua Caliente Debris Avalanche. The result was the formation of a horseshoe-shaped crater 600 m wide open to the northwest. Afterward, several undated effusive and explosive eruptions occurred. All these eruptions are likely Late Pleistocene to Holocene in age because the landforms derived of that activity overlap the horseshoe-shaped crater. To corroborate this hypothesis, we used surface exposure dating with *in situ*-produced cosmogenic ^{36}Cl combined with lichenometry and dendrochronology in the summit domes, the Ardillas dome, the horseshoe-shaped crater's cliff, and a lava. The ^{36}Cl exposure ages (9.3 ± 1.9 ka; 8.9 ± 0.9 ka; 8.6 ± 1.7 ka) of the summit domes are statistically indistinguishable within the associated uncertainties and suggest that the domes formed during Early Holocene. Instead, the southern part of the Late Pleistocene collapsed crater yielded significantly younger ages ranging from 5.3 ± 0.6 to 7.0 ± 0.8 ka. These ages are assumed to be minimum and might indicate later rockfall activity and instability, affecting the horseshoe-shaped crater. The ^{36}Cl exposure age of an andesitic lava (0.4 ± 0.1 ka), emplaced to the SW of Tacaná, is in good agreement with lichenometry (> 347 yr). These ages could represent a gravitational collapse event associated with phreatic explosions vented close to a scar collapse. The ^{36}Cl exposure ages derived from the Ardillas lava dome (0.3 ± 0.1 ka) do not correspond to its emplacement age. The dome must be older than pyroclastic deposits dated at 760 ± 30 yr BP (^{14}C) that cover its surface. Strikingly, the ^{36}Cl , lichenometrical and dendrochronological data of the “Andesitic” lava and the Ardillas dome are associated with NE-SW landslide scars, explosion craters, phreatic vents, fumarolic activity, and tensional fractures. All these features are perpendicular to the NW-SE minimum stress regime (σ_3), affecting the TVC and generating gravitational activity. Nowadays, gravitational collapses represent a real threat to the surrounding populations that can be triggered not only by volcanic activity but also by seismicity and extraordinary rains.

Key words: Tacaná, México, *in situ*-produced cosmogenic ^{36}Cl dating, lichenometry, dendrochronology, Holocene.

73

74 **1. Introduction**

75

76 Mexican volcanoes have experienced intensive activity during the Holocene, especially in
77 the Trans-Mexican Volcanic Belt, the Chiapanecan Volcanic Arc, the northwestern edge of
78 the Central American Volcanic Arc, Baja California (San Quintin volcanic fields), el
79 Pinacate Volcanic Field (NW Mexico) and the Revillagigedo Archipelago (700 km west of
80 Manzanillo city). Roughly 153 well-constrained Holocene eruptions have been reported of
81 which 63% were produced on active stratovolcanoes and calderas and 37% in monogenetic
82 volcanic fields (Macías and Arce, 2019). To constrain the chronology of these eruptions,
83 several dating methods such as radiocarbon, $^{40}\text{Ar}/^{39}\text{Ar}$, ^{230}U -Th in zircons, paleomagnetism
84 and *in situ*-produced cosmogenic ^{36}Cl and ^{10}Be have been used (Macías and Arce, 2019).
85 However, many deposits and landforms remain undated, resulting in limitations in the
86 chronological records that prevent establishing highly-resolved histories of volcanic
87 activity to anticipate future eruptions and assess the potential risks for neighboring
88 populations. Such limitations are encountered for Tacaná Volcanic Complex (TVC),
89 located in the State of Chiapas in southern Mexico and the San Marcos Department in
90 Guatemala. Today, more than 300,000 inhabitants live within a 35 km radius of the summit,
91 placing the TVC as the second most hazardous volcano in Mexico, just after Popocatepetl.

92

93 A phreatic explosion occurred at the TVC in 1986 after which it has been considered an
94 active volcano in a quiescent state. The main crater of Tacaná volcano has a horseshoe-
95 shaped crater associated with a collapse event that occurred 15 ± 5 ka ($^{40}\text{Ar}/^{39}\text{Ar}$) that
96 dispersed the Agua Caliente debris avalanche deposit (Macías et al., 2010). One of the
97 andesitic lavas (Agua Zarca) erupted 12 ± 5 ka ($^{40}\text{Ar}/^{39}\text{Ar}$) from the collapsed crater and
98 covered the debris avalanche (Macías et al. 2010). These ages are associated with large
99 uncertainties and therefore only provide an approximate chronology of the respective
100 events and tentatively bracket the volcano's subsequent activity. Besides, little is known
101 about its activity over the Holocene, especially the effusive activity, with several summit

102 landforms (i.e. domes, lavas) of unknown age. Here, we date four lava domes (three from
103 the Tacaná summit informally dubbed “East”, “Northwest” and “Southwest”, and the
104 Ardillas dome), the cliff of the horseshoe-shaped crater and a lava (informally named
105 “Andesitic lava”) extruded from the summit of Tacaná. We hypothesized that all these
106 landforms have a Late Pleistocene- Holocene age because they overlap the horseshoe-
107 shaped crater dated at 15 ± 5 ka ($^{40}\text{Ar}/^{39}\text{Ar}$). To confirm this hypothesis, we collected
108 eighteen samples from 5 cm flat-topped solid andesitic surface rocks for exposure dating
109 with *in situ*-produced cosmogenic ^{36}Cl (cosmic ray exposure; ^{36}Cl CRE hereafter) combined
110 with lichenometry and dendrochronology (Ardillas dome and the “Andesitic lava”). The
111 latter two methods provided minimum ages of the sampled rocks. To understand the
112 volcanic evolution of the TVC, we generated a geologic map and stratigraphy of the
113 summit area aided by new structural data. Finally, we performed whole-rock chemistry of
114 all samples to define their chemical composition and evolution of the summit structures.

115

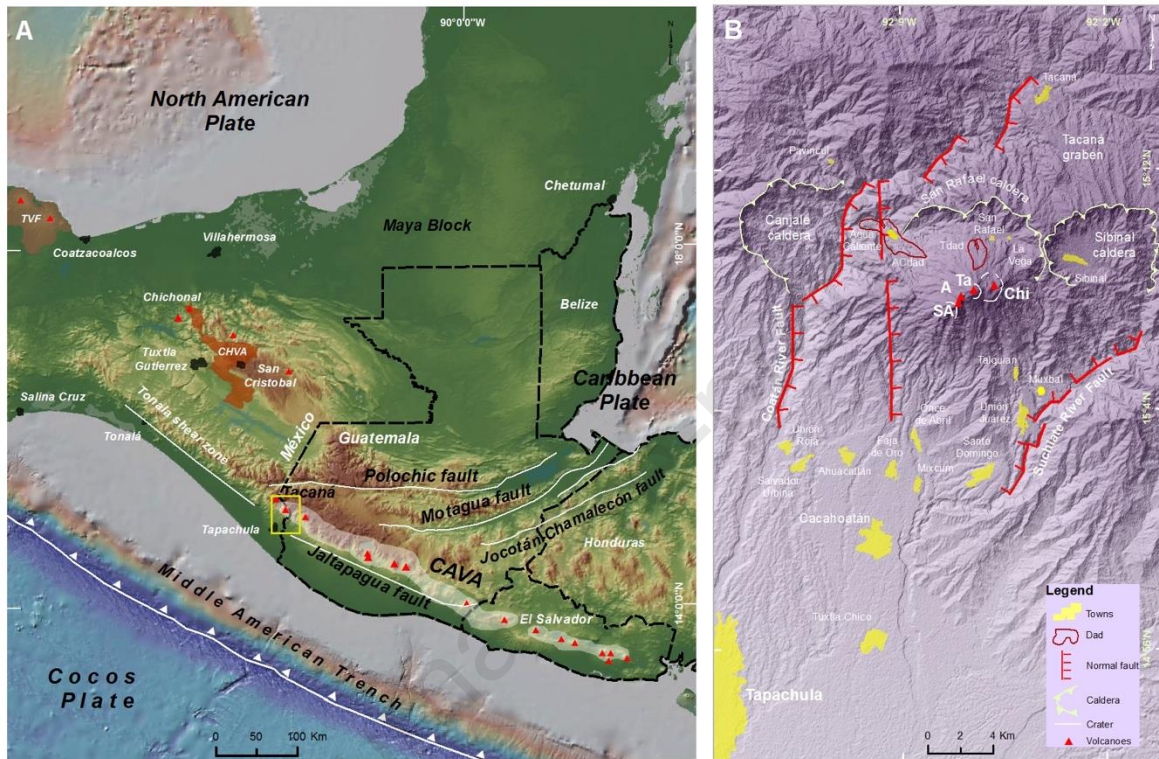
116 **2. Study area and previous work at Tacaná Volcanic Complex (TVC)**

117

118 The TVC is part of the northwestern end of the Central American Volcanic Arc (Fig. 1A).
119 The complex is constituted by four NE-SW aligned volcanic structures called Chichuj,
120 Tacaná, Ardillas Dome, and San Antonio (Fig. 1B) (García-Palomo et al., 2006). It was
121 built on Mesozoic metamorphic and Tertiary intrusive rocks (150 Ma and 35-13 Ma
122 respectively), and deposits from mid-Pleistocene calderas (1-2 Ma) (Garduño-Monroy et
123 al., 2015). The complex is affected by three fault systems, which are from older to younger:
124 NW-SE striking fractures and faults that cut the metamorphic and intrusive basement, NE-
125 striking faults parallel to the TVC, and the N-S striking youngest faults that are
126 superimposed on the others (García-Palomo et al., 2006). The NE-SW fault system delimits
127 the Tacaná graben that has controlled the emplacement and evolution of the Chichuj,
128 Tacaná, and San Antonio volcanoes and the Las Ardillas dome structures, as well as the
129 emplacement of Sibinal and San Rafael calderas (Fig. 1B). A linear regression of the
130 alignment of these structures showed an adjustment with a correlation coefficient (r) of

131 0.91, indicating that their location is controlled by N65°E orientation fissures defined by a
 132 minimum stress (σ_3) with a N53°W orientation (García-Palomo et al., 2006; Macías et al.,
 133 2010).

134



135

136

137 Figure 1. (A) Map showing the tectonic context of southern Mexico and the location of the Tacaná
 138 volcanic complex (TVC) (yellow rectangle). Abbreviations: CAVA, Central American Volcanic
 139 Arc; TVF, Tuxtla Volcanic Field; CHVA, Chiapanecan Volcanic Arc. (B) Detailed Digital
 140 Elevation Model of the TVC. Abbreviations: Chi (Chichuj), Ta (Tacaná), A (Ardillas dome) and SA
 141 (San Antonio) volcanoes; ACdad (Debris Avalanche Deposits of Agua Caliente) and Tdad (Debris
 142 Avalanche Deposits of Tuimanj). Main fault systems are displayed in red.

143

144 Volcanic activity in the TVC started ca. 300 ka ago with the emplacement of Chichuj
 145 volcano, followed by the emplacement of Tacaná structure around 40 ka (Limón-
 146 Hernández, 2011), and San Antonio volcano some ca. 20 ka. Finally, a lava dome defined
 147 as Ardillas (>800 yr) was emitted between San Antonio and Tacaná edifices. Since its
 148 formation, the TVC has produced several types of eruptions such as sector collapse (Macías
 149 et al., 2010), Peléean (Macías et al., 2000), Plinian and subplinian events (Arce et al.,

150 2012), and intense effusive activity (Limón-Hernández, 2011). As mentioned before, the
151 Tacaná summit has a 600 m wide horseshoe-shaped crater open to the northwest. This
152 crater was produced by a collapse 15 ± 5 ka ago ($^{40}\text{Ar}/^{39}\text{Ar}$) followed by the emplacement
153 of the Agua Caliente debris avalanche (Macías et al., 2010).

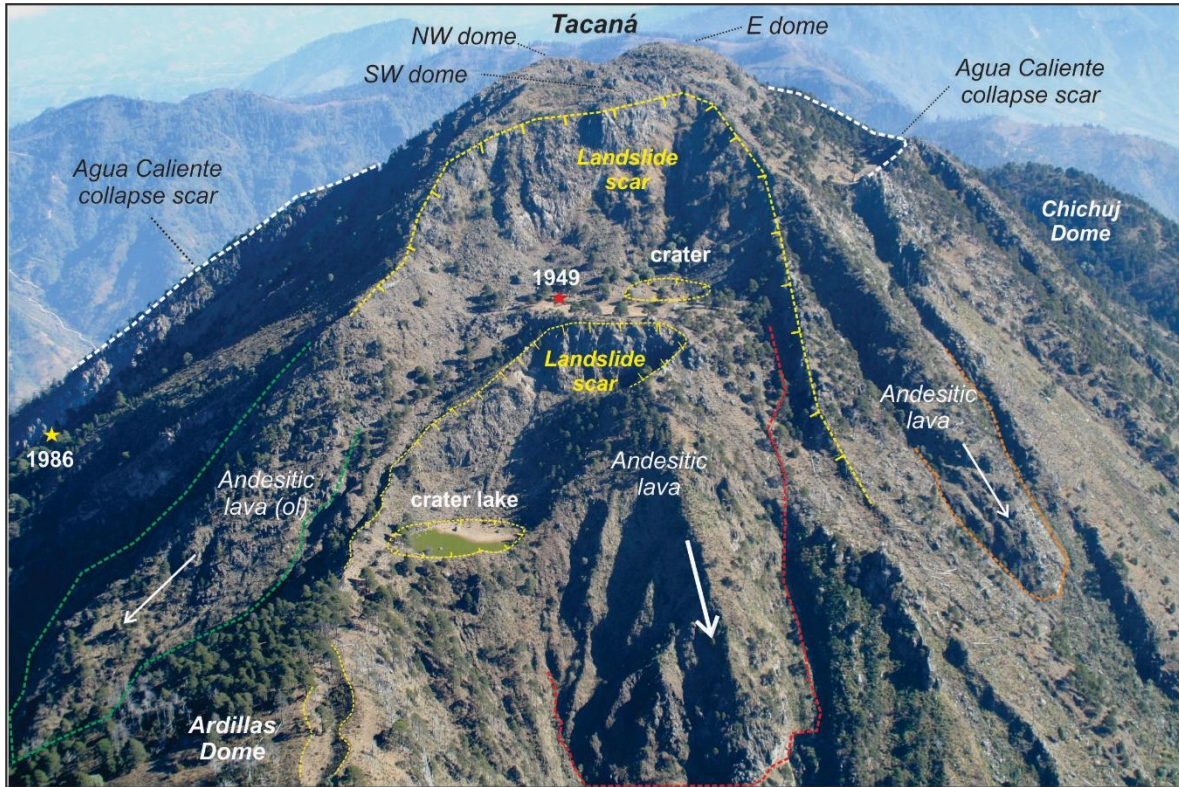
154

155 After the collapse, intense effusive activity took place inside the horseshoe-shaped crater
156 through the emission of several lava flows to the NW. One of these lavas called Agua Zarca
157 was dated at 12 ± 5 ka ($^{40}\text{Ar}/^{39}\text{Ar}$) (Macías et al. 2010). Subsequent lava emissions infilled
158 the horseshoe-shaped crater and extruded the three bulb-like domes (“East”, “Northwest”,
159 and “Southwest”) at the summit of Tacaná (Figs. 2 and 3). Prior or during the first stages of
160 the extrusion of these domes, an olivine-bearing lava flow was emitted to the southwest of
161 Tacaná (green dashed line in Fig. 2). Another lava of andesitic composition was emitted to
162 the southwest between the ca. 15 ka horseshoe-shaped crater and the Ardillas Dome (red
163 dashed line in Fig. 2). These lavas and associated domes have not been dated yet and
164 therefore their relationship with the TVC Holocene eruptive stratigraphy has not been
165 determined. As revealed by stratigraphy and radiocarbon dating, at the beginning of the
166 Holocene an explosive eruption called Once de Abril disrupted the summit of Tacaná,
167 dispersing dense and dilute Pyroclastic Density Currents (PDCs) that swept the volcano
168 flanks beyond the break in slope (Macías et al., 2015). Around the same time, the northern
169 part of Tacaná collapsed producing the Tuimanj debris avalanche towards Guatemala
170 (Limón-Hernández, 2011). Since then, the TVC has generated at least nine radiocarbon
171 dated smaller eruptions that have dispersed pyroclastic deposits on the middle and upper
172 flanks of the complex dated at ca. 7.6, ca. 6.1-5.6, ca. 2.6, ca. 1.9, ca. 0.9, ca. 0.8, ca. 0.37,
173 ca. 0.28, and ca. 0.15 ka (Macías et al., 2015).

174

175

176

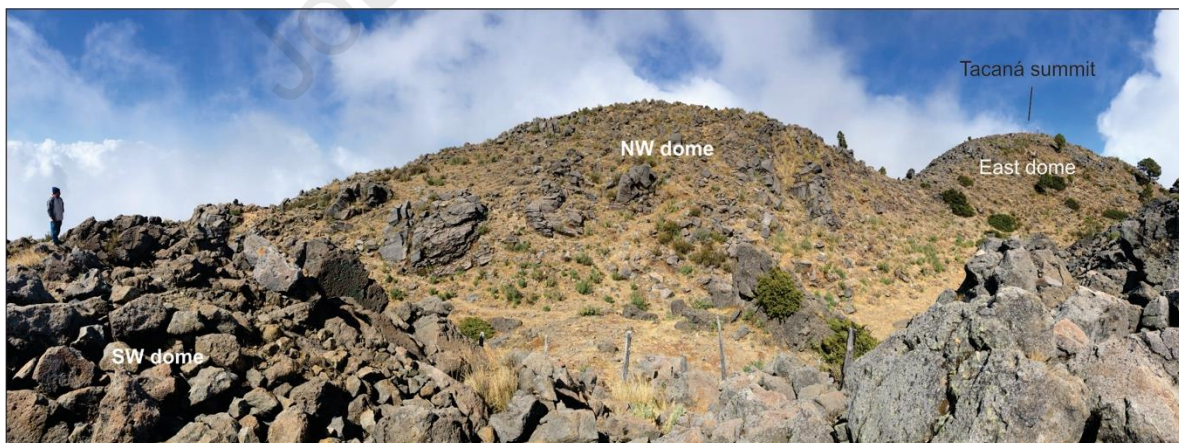


177

178

179 Figure 2. Aerial view from the southwest of the TVC, showing the summit of Tacaná volcano.
 180 Notice the Agua Caliente collapse scar (ca. 15 ka), two explosion craters, and two landslide scars
 181 (yellow dashed lines). The stars point out the locations of the 1949 (red) and 1986 (yellow) phreatic
 182 explosions. The white arrows indicate the flow direction of the andesitic lava analyzed in this study.

183



184

185 Figure 3. Detailed photograph of East, Northwestern and Southwestern lava domes from the summit
 186 of Tacaná volcano.

187

188 The precise source of these eruptions is not known yet because the summit has been
189 modified by neotectonics and mass wasting processes. In fact, two NE-SW landslide scars
190 can be recognized at Tacaná (Figs. 2 and 4), one of them is 350 m wide and affects the
191 summit domes; and the second one is 60 m wide and affects the “Andesitic lava” located
192 between the Ardillas dome and the horseshoe-shaped crater, southwest of the summit.
193 Another two NW-SE collapses affect the northwestern part of the Tacaná cone. At least two
194 of the Late Holocene eruptions have occurred along the NE-SW fractures between Tacaná
195 and Las Ardillas dome (Fig. 4). A phreatomagmatic eruption at 760 ± 30 yr cal BP
196 dispersed dilute PDCs and ash fallouts generating a 80 x 60 m wide crater that today
197 contains a greenish lake (Macías et al., 2018). Northeast of this crater lake, at the base of
198 the largest NE-SW scar, another explosion crater vented on top of the “Andesitic lava”.
199 This 60 x 25 m wide crater is made of around 5 m thick breccia interbedded with
200 discontinuous pyroclastic deposits (Fig. 2). The 1949 phreatic explosion of Tacaná
201 (Mülleried, 1951) was vented between these two explosion craters and along the NE-SW
202 fractures.

203

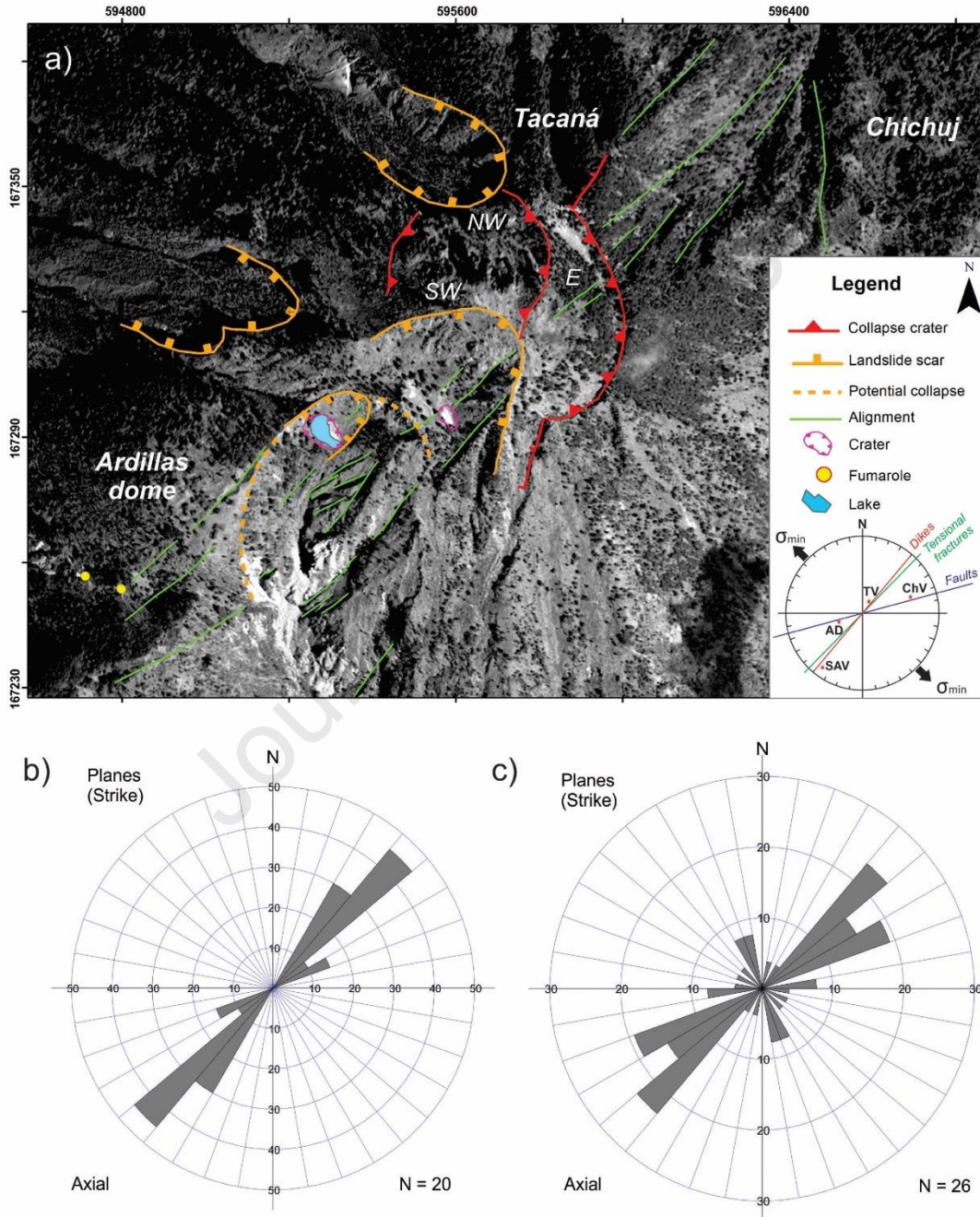
204 In 1986, Tacaná resumed activity with another phreatic explosion at the base of a lava cliff,
205 which had formed during the ca.15 ka collapse of Tacaná (Fig. 2). This explosion attracted
206 the attention of scientists (Martini et al., 1987; De la Cruz-Reyna et al., 1989) leading to the
207 discovery of past eruptions (Espíndola et al., 1989) and rise up the awareness of the danger
208 that the volcano represented to the surrounding communities. As a consequence, Mercado
209 and Rose (1992) presented the first general hazards map and mentioned historic reports of
210 another eruption that had occurred around 1855-1856. This eruption has recently been
211 related with the suppression of tree-ring growth between 1857 and 1868 (Carlón et al.,
212 2020).

213

214 Today, the TVC shows signs of volcanic activity with fumaroles on the northwestern flank
215 of San Antonio volcano and thermal springs and fumaroles output on the northwestern
216 flank of Tacaná, which reach as far as the village of Agua Caliente (Rouwet et al., 2004;

217 2009). On top of the Tacaná summit domes (“East”, “Northwest” and “Southwest”), a
 218 paleosol is covered by the 1902 ash fall deposits of Santa Maria volcano, Guatemala
 219 (Williams and Self, 1983).

220



221

222 Figure 4. a) Structural map of the TVC summit, b) Rose diagram obtained from the SPOT 7 image
 223 and the DEM; c) Rose fracture of the data collected along the NE-SW fracture on top of the San
 224 Antonio dome. Dome abbreviations are: E = Eastern, NW = Northwestern, and SW = Southwestern.

225

226 **3. Methods**

227

228 **3.1. Stratigraphical and structural analyses**

229

230 The stratigraphic and structural analyses of the area were carried out with a SPOT 7
231 satellite image, a high resolution Digital Elevation Model (5 m resolution), two Digital
232 Elevation Model (12.5 m resolution, Alospolar, NASA; and 100 m resolution,
233 GeoMapApp.org), and the collection of field data gathered during 2018 and 2019 (Fig. 4a).
234 In specific locations, stratigraphic sections were reconstructed and samples were collected
235 for different analysis.

236

237 **3.2. Whole-rock chemistry**

238

239 In this paper, six new chemical analyses for Tacaná summit domes and lavas are reported.
240 Samples were cleaned and washed, then pulverized with a stainless steel mortar. Powder
241 samples were analyzed by the X-ray Fluorescence (XRF) method at Service d'Analyse des
242 Roches et des Minéraux (SARM, CRPG, Nancy, France), major elements by ICP-OES, and trace
243 elements by ICP-MS except Cl (spectrophotometry), B (colorimetry) and Li (atomic absorption).
244 Loss on ignition (LOI) was determined for all analyzed samples, for which 1 gram of
245 powder was heated at 1000°C for one hour and then reweighed.

246

247 **3.3. Lichenometry**

248

249 Lichenometry used in this study provides a minimum age of the “Andesitic lava” and the
250 Ardillas dome. The largest diameter of the biggest circular thalli of *Rhizocarpon*
251 *geographicum* located on well preserved protruding features with smooth surfaces were
252 measured using a Bernier calibrator. Digital photographs of the lichen were taken, using a
253 scale (one peso coin of 21 mm of diameter). The age of the largest lichen was determined
254 applying the growth rate of 0.23 mm a⁻¹ for *Rhizocarpon geographicum* constrained on
255 Iztaccíhuatl volcano, situated ca. 900 km to the northwest of the TVC (Palacios et al.,
256 2012). Despite the distance, the measurement sites of the lichen are located at a similar

257 altitude (~4,000-4,500 m a.s.l.), and climate at that altitudinal range is not significantly
258 different on both volcanoes.

259 **3.4. Dendrochronological sampling and sample processing**

260 Dendrochronological samples were collected from *Pinus hartwegii* Lindl (9 samples) and
261 *Juniperus monticola* (1 sample) on the summits of the Tacaná volcano and Ardillas dome in
262 the years 2017 and 2019. No samples of trees were collected on the “Andesitic lava”,
263 because continuous landslides limit their colonization. The sampled trees were located at
264 elevations ranging from 3400 to 4040 m. The sampling consisted in extracting two or three
265 increment cores from each tree using a Höglof borer (10 mm diameter; Höglof Sweden AB,
266 Långsele, Västernorrland, Sweden) perpendicular to the stem and at breast height (1.30 m).
267 Then, 10 trees were drilled for a total sampling set of 22 increment cores. Increment cores
268 were processed using sandpaper with progressive grain sizes from 80 to 1200 grains·cm⁻²
269 according to standard dendrochronological techniques (Stokes and Smiley, 1996). Once the
270 annual rings were visible, growth rings were counted from the pit to the bark under the
271 microscope.

272 273 **3.5. Cosmic ray exposure dating with ³⁶Cl**

274
275 In Mexico, CRE dating has been previously used to determine the age of lavas (Vázquez-
276 Selem and Heine, 2011; Alcalá-Reygosa et al., 2018 a, b) and domes (Arce et al., 2003) in
277 stratovolcanoes and monogenetic edifices. CRE dating relies on the interaction of cosmic
278 ray derived particles with certain target elements of the rocks. ³⁶Cl can be extracted from
279 any mineral phase and rock type that contains one or more of its most important target
280 elements, i.e. Ca, K and Cl (Dunai, 2010). Moreover, it has been recently demonstrated that
281 ³⁶Cl dating provides surface exposure ages of volcanic rocks of as young as a few hundred
282 years (Jomelli et al., 2016).

283 284 **3.5.1. Sampling and physical treatment of the samples**

285
286 Eighteen samples (Tac 1 - Tac 18) were taken with hammer and chisel from the 5 cm flat-
287 topped solid rock surfaces (Table 1). Twelve of them were collected on the “East”,
288 “Northwest” and “Southwest” Tacaná domes (Tac 1 - Tac 9) and the Ardillas dome (Tac 13
289 - Tac 15). Three samples were taken from the limit of the steep cliff of the horseshoe-

290 shaped crater (Tac 10 - Tac 12) and another three come from the “Andesitic lava” located
 291 to the southwest of this crater (Tac 16 - Tac 18). All the samples were collected from well-
 292 preserved surfaces without evidence of erosion, weathering or boulder toppling to minimize
 293 potential bias in the ^{36}Cl surface concentrations, which accumulated during exposure to
 294 cosmic rays since formation of the sampled surfaces (Alcalá-Reygosa et al., 2018a).
 295 Furthermore, samples were collected from protruding geometries to minimize the effects of
 296 surface shielding by pyroclastic layers and soils. The geographic coordinates were obtained
 297 with Garmin GPS, and the topographic shielding was determined with compass and
 298 clinometer. It must be noted that the samples taken from the steep cliff of the horseshoe-
 299 shaped crater, Las Ardillas dome and the “Andesitic lava” represented a challenge due to
 300 active gravitational processes, neotectonics and slope instability, which could compromise

301 our original
 302 plan to determine
 303 the ages of the

Sample	Latitude (°N)	Longitude (°W)	Altitude (m.a.s.l)	Thickness (cm)	Shielding factor
Tac 1	15.13	-92.10	4086	2.0	0.98665
Tac 2	15.13	-92.10	4097	2.0	0.99343
Tac 3	15.13	-92.10	4102	2.5	0.97627
Tac 4	15.13	-92.10	4081	4.0	0.99637
Tac 5	15.13	-92.10	4088	2.0	0.99718

304 landforms.

305	Tac 6	15.13	-92.10	4081	2.0	0.97541
306	Tac 7	15.13	-92.10	4079	2.5	0.99977
	Tac 8	15.13	-92.10	4077	2.0	0.99687
307	Tac 9	15.13	-92.10	4089	2.5	0.99858
308	Tac 10	15.13	-92.10	3958	1.5	0.99129
	Tac 11	15.13	-92.10	3986	1.5	0.98564
309	Tac 12	15.13	-92.10	3995	1.5	0.95418
310	Tac 13	15.12	-92.11	3792	1.5	0.95905
	Tac 14	15.12	-92.11	3764	1.5	0.98316
311	Tac 15	15.12	-92.11	3755	1.0	0.97223
312	Tac 16	15.12	-92.11	3898	1.5	0.92531
	Tac 17	15.13	-92.11	3887	1.5	0.95965
313	Tac 18	15.13	-92.11	3929	3.0	0.87414

314

315

316

317

318

319

320 Table 1. Field data and characteristics of rock samples from lava domes, cliff horse-shoe shaped
 321 crater and lava from Tacaná volcano, used for the ^{36}Cl CRE dating calculations. The shielding
 322 factor was obtained using the Topographic Shielding Calculator v2.0 provided by CRONUS-Earth
 323 Project (2014).

324

325 At Instituto de Geofísica (Unidad Morelia; Universidad Nacional Autónoma de México),
 326 lichens, mosses and other organic matter were removed from the samples with a brush and
 327 then they were crushed with a roller grinder and sieved to retrieve the grain size fraction
 328 (0.25-0.50 mm). Once the crushed samples shipped to the Centre Européen de Recherche et
 329 d'Enseignement des Géosciences de l'Environnement (CEREGE; France), aliquots of the
 330 bulk rock were first taken for the analysis of the major and trace element concentrations at
 331 the "Service d'Analyse des Roches et des Minéraux" (SARM, CRPG, Nancy, France),
 332 which are needed to estimate the samples ^{36}Cl production rate from the capture of the low-
 333 energy neutrons by Cl in the samples (Table 2). This specific ^{36}Cl production reaction is
 334 difficult to constrain and associated with significant uncertainties (Schimmelpennig et al.,
 335 2009). As feldspar phenocrysts often contain significantly less Cl than volcanic whole rock

336 samples (Schimmelpfennig et al., 2009), the proportion of the non-magnetic feldspar in the
337 fraction of the sample grains used for ^{36}Cl extraction was increased by discarding the most
338 magnetic minerals with a magnetic separator “Frantz LB-1” at CEREGE. However,
339 because feldspars were not abundant enough, pure feldspar was not used to avoid the risk of
340 too small sample masses with ^{36}Cl contents below the detection limit.

341

342 **3.5.2. Chemical sample treatment and measurement**

343

344 Between 20 and 100 g of the feldspar-enriched sample fractions (Tac 1 - Tac 18) were
345 treated for ^{36}Cl extraction following the method described in Schimmelpfennig et al.
346 (2011). The samples were washed in ultrapure water to remove fine-grained powder and
347 then leached in a dilute HF/HNO₃ mixture to dissolve 15 - 20 % of the initial sample mass.
348 Thus, the samples were decontaminated from atmospheric ^{36}Cl and potentially Cl-rich
349 groundmass grains were reduced (Schimmelpfennig et al., 2009). Then, the samples were
350 dried and 2 g aliquots of each sample were put aside for analysis of the major elements at
351 SARM, because Ca, K, Ti, and Fe are the target elements for spallogenic/muogenic
352 production of ^{36}Cl (Table 3). The following steps consisted in adding a ^{35}Cl -enriched spike
353 (~ 99%) to each sample and dissolving totally them in a HF/ HF/HNO₃ mixture. A
354 chemistry blank was processed following the same protocol as the samples.

355

356 After total dissolution, the samples were centrifuged to discard the undissolved residues
357 and gel (fluoride complexes, CaF₂). Then, chlorine in the liquid solution was precipitated to
358 silver chloride (AgCl) by adding 2 ml of a silver nitrate (AgNO₃) solution at 10%. To allow
359 the AgCl to settle down on the bottom of the bottles, samples were stored for 2 days in a
360 dark place. This enabled the extraction of the supernatant solution (excess HF and HNO₃)
361 by a peristaltic pump avoiding the disturbance of the AgCl precipitate. In the next step,
362 aiming to reduce the isobaric interferences of ^{36}S throughout the ^{36}Cl measurements by
363 Accelerator Mass Spectrometry (AMS), sulphur was removed in the form of barium
364 sulphate (BaSO₄) obtained after the re-dissolution of this first AgCl precipitate and the
365 addition of 1 ml of a saturated solution of barium nitrate (Ba(NO₃)₂). BaSO₄ was discarded
366 by centrifuging and filtering the supernatant with a syringe and an acrodisc filter. Then,

367 AgCl was precipitated again with 3-4 ml of diluted HNO₃ (1:1 vol.). The precipitate was
368 collected after centrifuging, was rinsed and finally dried in the oven at 80 °C for 2 days, and
369 later loaded into nickel cathodes for measurements of the ³⁶Cl/³⁵Cl and ³⁵Cl/³⁷Cl ratios by
370 AMS isotope dilution at the French national AMS facility ASTER (CEREGE, France)
371 (Arnold et al., 2013), which took place in 2019. The ³⁶Cl/³⁵Cl ratio was normalized to in-
372 house standard SM-CL-12 with an assigned ³⁶Cl/³⁵Cl ratio of (1.428 ± 0.021) ×10⁻¹²
373 (Merchel et al., 2011), and regarding the ³⁵Cl/³⁷Cl ratio, a natural ratio of 3.127 was
374 assumed. The AMS analytical data is given in Table 4.

375

376 **3.5.3. *In situ*-produced ³⁶Cl age calculation**

377

378 We calculated the ³⁶Cl CRE ages using the Excel spreadsheet published by
379 Schimmelpfennig et al. (2009). We used the following ³⁶Cl production rates and parameters
380 referenced to sea level and high latitude based on the time-invariant “St” scaling (Stone,
381 2000): 42.2 ± 4.8 atoms ³⁶Cl (g Ca)⁻¹ yr⁻¹ for spallation of Ca (Schimmelpfennig et al.,
382 2011); 148.1 ± 7.8 atoms ³⁶Cl (g K)⁻¹ yr⁻¹ for spallation of K (Schimmelpfennig et al.,
383 2014); 13 ± 3 atoms ³⁶Cl (g Ti)⁻¹ yr⁻¹ for spallation of Ti (Fink et al., 2000); 1.9 ± 0.2 atoms
384 ³⁶Cl (g Fe)⁻¹ yr⁻¹ for spallation of Fe (Stone et al., 2005), and 696 ±185 neutrons (g air)⁻¹ yr⁻¹
385 ¹ at the Earth’s surface/atmosphere interface for the production rate of epithermal neutrons
386 from fast neutrons in the atmosphere (Marrero et al., 2016). Both the nucleogenic and
387 muonic scaling factors were determined using the time-invariant scaling model of Stone
388 (2000) based on CosmoCalc (Vermeesch, 2007) and the atmosphere standard model
389 (N.O.A.A., 1976). High-energy neutron attenuation length of 160 g cm⁻² was used. A
390 density of 2.5 g/cm³ is assumed for all samples.

391

392 The topographic shielding factor was estimated applying the Topographic Shielding
393 Calculator v2.0 provided by CRONUS web calculator. The ³⁶Cl CRE ages are presented
394 without erosion and snow cover corrections. Regarding erosion, all the sampled surfaces
395 are well-preserved whereas potential snow cover effects were not considered because
396 snowfall is very rare in this tropical climate.

397

398 4. Results

399

400 4.1. Structural setting and stress regime

401

402 The structural data is presented in figure 4a and plotted in rose diagrams on figures 4b-c.

403 The performed image analyses and field reconnaissance revealed the occurrence of

404 elongated rhombic large scale fractures on top of Las Ardillas dome with a preferential

405 direction between N30°E to N70°E (Figs. 2 and 4b). These fractures have a NE-SW main

406 axis. Their SW tip ends in a hydrothermal alteration zone with fumaroles on the northern

407 flank of San Antonio volcano and their NE tip is connected with the two NE-SW landslide

408 scars. Along these rhombic fractures occurred the 1949 phreatic explosion, signs of

409 hydrothermal fluid paths, and the two explosion craters described in figures 2 and 4. The

410 structural analysis of field data in andesitic rocks shows a preferential fracturing system

411 with a N40°E to N70°E orientation and a secondary one with NNW-SSE direction (Fig.

412 4c). Analysis of all these data allows defining a stress regime atop the TVC represented by

413 a minimum main stress (σ_3) with a N40°W \pm 10° orientation.

414

415

416

417

418 4.2. Cosmogenic ^{36}Cl chronology, lichenometry and dendrochronology.

419

420 In Table 4, the ^{36}Cl CRE ages are given with their full uncertainties, i.e. including

421 analytical and production rate errors, as well as with their analytical errors only. In the text

422 and figures, individual sample ages are shown with their analytical errors only, while

423 arithmetic mean ages are given with their standard deviations. The age population from

424 each dated volcanic feature was tested for outliers using the χ^2 test of Ward and Wilson

425 (1978). The individual ^{36}Cl ages range between 11.0 ± 1.8 ka and 170 ± 70 years. Most of

426 the sample fractions that were little enriched in feldspar (see section 3.5.1), have high

427 natural Cl concentrations (up to ~265 ppm), while Cl concentrations as low as 13 ppm were

428 obtained in sample fractions with a high feldspar proportion. This led to ~10-65%

429 contributions from Cl-derived ^{36}Cl to the total ^{36}Cl production and associated uncertainties
 430 in resulting ages of up to ~22% (Table 2 and 3).

431

432 **4.2.1. Tacaná summit domes**

433

434 The summit “East”, “Northwest” and “Southwest” lava domes are hosted within the 600 m
 435 wide horseshoe-shaped crater of Tacaná that is breached to the northwest (Figs. 2 and 3).
 436 They have a bulby shape, with three recognizable lobes. Together these domes occupy an
 437 area of 0.18 km², with a radius of approximate 300 m, and correspond to a volume of 0.017
 438 km³. The highest dome (“East dome”) has an elevation of 4060 m a.s.l. It rises 87 m above
 439 the surrounding terrain and holds an older microwave antenna. This dome is separated from
 440 the “Northwest” and “Southwest” domes by a N-S fault scar. The western lava lobes reach
 441 a maximum elevation of 3990 m and they are not easily distinguished from the Eastern
 442 dome.

443

444 The summit of the “Northwest” and “Southwest” domes are separated by a 15 m depression
 445 in north-south direction. The “Southwest” dome emplaced an olivine-bearing lava to the
 446 southwest, and both are affected by the large NE-SW scar open to the southwest. The
 447 “Southwest” and the “Northwest” domes have an andesitic composition of 62.48 wt.% SiO₂
 448 and 62.65 wt.% SiO₂, respectively. A dacitic composition with 63.6 wt.% SiO₂ (on
 449 anhydrous basis) has been evidenced on the “East” dome (Fig. 5a). The olivine-bearing
 450 lava is the most mafic lava analyzed. It is andesitic in composition (Fig. 5a) with 57.5 wt.%
 451 SiO₂ that falls close to the basaltic andesitic field.

452

Sample	Samples calculated with this composition	Unit	SiO ₂	TiO ₂	Al ₂ O ₃	Fe ₂ O ₃	MnO	MgO	CaO	Na ₂ O	K ₂ O	P ₂ O ₅	LOI	Total	Li	Sm	Gd	Cl	U	Th
*Tac0911	-	PreCL	60.27	0.64	17.11	6.48	0.11	2.36	5.98	3.78	2.23	0.17	0.27	99.40	-	-	-	-	-	3
*Tac0808	-	AndL	59.51	0.66	18.03	6.54	0.12	2.67	6.23	3.64	2.08	0.19	0.23	99.90	-	-	-	-	-	4
*Tac0829E	-	ME	53.69	0.95	18.56	8.53	0.12	4.06	8.36	3.58	1.23	0.20	0.21	99.49	-	-	-	-	-	3
*Tac0829L	-	AndL	61.13	0.57	16.83	5.73	0.10	2.42	5.62	3.71	2.23	0.15	1.38	99.87	-	-	-	-	-	4
*Tac0829a	-	AndL	62.27	0.59	16.83	5.60	0.10	2.21	5.40	3.80	2.32	0.16	0.35	99.63	-	-	-	-	-	4

Sample		CaO (%)	K ₂ O (%)	TiO ₂ (%)	Fe ₂ O ₃ (%)	SiO ₂ (%)	Na ₂ O (%)	MgO (%)	Al ₂ O ₃ (%)	MnO (%)											
*Tac0827	-	PreCL	58.70	0.61	16.67	6.15	0.11	2.52	5.70	3.62	2.13	0.16	3.23	99.60	-	-	-	-	-	-	4
*Tac0823	-	And-Ol	57.28	0.80	17.74	7.25	0.11	3.88	7.21	3.59	1.68	0.17	0.08	99.79	-	-	-	-	-	-	3
*Tac0809	-	Dome	60.77	0.64	17.38	6.23	0.11	2.63	5.96	3.69	2.15	0.17	0.23	99.96	-	-	-	-	-	-	3
*Tac0811	-	Dome	62.61	0.56	16.69	5.57	0.10	2.30	5.41	3.69	2.38	0.16	0.24	99.71	-	-	-	-	-	-	3
**Tac9878	-	Dome	62.78	0.55	16.88	5.26	0.10	2.17	5.34	3.70	2.32	0.15	0.80	100.05	-	-	-	-	-	-	-
***Tac9863	-	ArD	62.96	0.58	16.76	4.82	0.11	2.42	5.74	3.82	2.06	0.13	0.60	100.00	-	4.2	-	-	-	2.8	4.7
¹ TAC-1	Tac 2, 3	Dome	61.25	0.62	16.22	6.05	0.11	2.46	5.22	3.65	2.31	0.15	1.12	99.16	24	3.3	2.8	300	1.4	4.35	
¹ TAC-4	Tac 5, 6	Dome	61.98	0.62	15.50	6.08	0.11	2.52	4.72	3.52	2.27	0.13	1.96	99.40	24	3.2	2.7	280	1.4	4.28	
¹ TAC-7	Tac 8, 9	Dome	61.42	0.61	16.16	5.75	0.11	2.59	5.28	3.62	2.34	0.14	1.34	99.36	25	3.1	2.7	370	1.5	4.23	
¹ TAC-10	Tac 11, 12	PreCL	61.16	0.64	16.19	6.80	0.13	2.41	5.07	3.59	2.38	0.17	0.65	99.19	21	3.1	2.7	72	1.5	4.16	
¹ TAC-13	Tac 14, 15	ArD	64.53	0.53	15.75	5.07	0.10	2.07	4.52	3.74	2.72	0.14	0.44	99.61	25	2.9	2.5	335	1.7	5.01	
¹ TAC-16	Tac 17, 18	AndL	64.36	0.51	15.83	4.72	0.09	1.87	4.55	3.73	2.65	0.14	0.72	99.16	24	2.8	2.4	320	1.7	5	

453 Table 2. Major and trace element concentrations in bulk rock samples from Tacaná Volcanic
454 Complex, before chemical treatment (see methods). We used the composition of one sample per
455 landform for the age calculations of all other samples from the same feature, assuming that
456 variations in compositions are insignificant. LOI, loss on ignition; total Fe as Fe₂O₃. Compiled
457 samples from Tacaná summit: *Limón-Hernández (2009). Units are: PreCL, Pre-collapse lava;
458 AndL, Andesitic lava; ME, Mafic enclave; And-Ol, olivine-bearing andesitic lava; ArD, Ardillas
459 dome. References: **Mora et al. (2004); ***García-Palomo et al. (2006); ¹This work.

Eastern lava dome									
Tac 1	6.08 ± 0.30	1.94 ± 0.10	0.32 ± 0.08	3.07 ± 0.46	62.71	4.04	2.12	18.09	0.08
Tac 2	5.52 ± 0.28	1.78 ± 0.17	0.26 ± 0.05	2.54 ± 0.38	65.35	3.66	1.68	16.60	0.07
Tac 3	6.21 ± 0.31	1.90 ± 0.40	0.31 ± 0.07	2.98 ± 0.45	62.49	4.09	2.10	18.38	0.08
Northwestern lava dome									
Tac 4	8.33 ± 0.42	0.60 ± 0.12	0.06 ± 0.02	0.65 ± 0.09	60.40	4.59	0.21	22.66	0.02
Tac 5	6.38 ± 0.32	1.43 ± 0.28	0.22 ± 0.05	2.05 ± 0.31	63.36	3.89	1.43	18.31	0.06
Tac 6	6.75 ± 0.33	1.32 ± 0.13	0.21 ± 0.05	2.18 ± 0.33	61.63	4.11	1.41	19.58	0.06
Southwestern lava dome									
Tac 7	9.14 ± 0.46	0.60 ± 0.15	0.05 ± 0.01	0.58 ± 0.09	57.21	5.25	0.18	25.29	0.02
Tac 8	6.41 ± 0.32	1.82 ± 0.36	0.29 ± 0.07	2.53 ± 0.38	62.07	4.18	1.76	18.69	0.07
Tac 9	6.78 ± 0.34	1.66 ± 0.33	0.25 ± 0.06	2.20 ± 0.33	61.66	4.38	1.62	19.77	0.06
Cliff horse-shoe shaped crater									
Tac 10	6.76 ± 0.34	1.47 ± 0.29	0.24 ± 0.05	2.73 ± 0.41	61.68	4.21	1.27	19.86	0.07
Tac 11	9.52 ± 0.48	0.45 ± 0.09	0.04 ± 0.01	0.54 ± 0.08	57.43	5.15	0.08	25.73	0.02
Tac 12	6.82 ± 0.34	1.33 ± 0.26	0.19 ± 0.05	2.64 ± 0.40	62.23	4.11	1.77	19.63	0.08
Ardillas lava dome									
Tac 13	7.44 ± 0.37	1.37 ± 0.18	0.23 ± 0.06	2.16 ± 0.22	60.37	4.50	1.54	21.05	0.06
Tac 15	6.71 ± 0.33	1.69 ± 0.17	0.26 ± 0.06	2.47 ± 0.25	61.95	4.33	1.79	19.79	0.07
Andesitic lava									
Tac 16	7.43 ± 0.37	1.32 ± 0.13	0.24 ± 0.06	2.14 ± 0.21	60.52	4.51	1.50	21.06	0.06
Tac 17	7.32 ± 0.37	1.35 ± 0.13	0.34 ± 0.08	3.29 ± 0.33	59.43	4.24	2.47	19.64	0.09
Tac 18	7.46 ± 0.37	1.28 ± 0.13	0.20 ± 0.05	1.94 ± 0.19	59.97	4.55	1.32	21.21	0.05

460 Table 3. Concentrations of the major elements, including the ³⁶Cl target elements Ca, K, Ti and Fe,
461 measured in splits taken from the samples after magnetic separation and the chemical pre-treatment.
462 Analyses carried out at Service d'Analyse des Roches et des Minéraux (SARM, CRPG, Nancy,
463 France) by ICP-OES.

464

465

466

467

468

Sample	Sample weight (g)	Mass Cl (mg) added by spike	$^{35}\text{Cl} / ^{37}\text{Cl}$	$^{36}\text{Cl} / ^{35}\text{Cl} (10^{14})$	Cl (ppm)	^{36}Cl conc (10^3 at g^{-1})	^{36}Cl age (ka)
Eastern lava dome							
Tac 1	66.87	2.016	3.595 ± 0.043	26.9 ± 1.4	265 ± 38	1060 ± 150	$9.7 \pm 2.1 (1.4)$
Tac 2	76.12	2.009	3.712 ± 0.045	21.9 ± 1.3	185 ± 25	621 ± 80	$7.3 \pm 1.5 (1.0)$
Tac 3	79.13	2.013	3.524 ± 0.042	31.5 ± 1.7	263 ± 40	1210 ± 180	$11.0 \pm 2.5 (1.8)$
Northwestern lava dome							
Tac 4	25.77	2.010	8.53 ± 0.10	21.6 ± 1.3	57 ± 7	449 ± 32	$9.7 \pm 1.4 (1.0)$
Tac 5	59.54	2.012	3.841 ± 0.046	22.4 ± 1.2	194 ± 25	690 ± 82	$8.0 \pm 1.6 (1.1)$
Tac 6	40.6	2.018	4.574 ± 0.054	23.4 ± 1.3	140 ± 17	622 ± 61	$8.9 \pm 1.6 (1.0)$
Southwestern lava dome							
Tac 7	19.7	2.019	8.66 ± 0.53	18.8 ± 2.0	73 ± 11	507 ± 60	$9.8 \pm 1.7 (1.3)$
Tac 8	82.81	2.003	3.625 ± 0.043	20.6 ± 1.2	200 ± 28	615 ± 84	$6.7 \pm 1.4 (1.0)$
Tac 9	60.73	2.013	3.736 ± 0.044	27.0 ± 1.4	224 ± 30	931 ± 115	$9.4 \pm 2.0 (1.3)$
Cliff horse-shoe shaped crater							
Tac 10	55.27	2.019	9.62 ± 0.11	22.4 ± 1.3	22 ± 3	205 ± 14	$5.29 \pm 0.72 (0.64)$
Tac 11	14.68	2.015	34.75 ± 0.43	1.08 ± 0.20	13 ± 2	22.2 ± 6.5	$0.66 \pm 0.21 (0.20)$
Tac 12	58.8	2.009	7.109 ± 0.084	26.8 ± 1.4	34 ± 4	276 ± 20	$6.99 \pm 0.95 (0.81)$
Ardillas lava dome							
Tac 13	69.06	2.056	3.789 ± 0.045	0.88 ± 0.20	185 ± 24	24.2 ± 6.3	$0.339 \pm 0.102 (0.099)$
Tac 14	30.79	2.008	10.60 ± 0.13	0.140 ± 0.063	33 ± 4	-	-
Tac 15	63.5	2.022	3.866 ± 0.046	0.46 ± 0.15	177 ± 23	11.8 ± 4.4	$0.169 \pm 0.069 (0.065)$
Andesitic lava							
Tac 16	50.98	2.043	4.078 ± 0.048	1.18 ± 0.24	172 ± 22	32.9 ± 7.8	$0.47 \pm 0.13 (0.11)$
Tac 17	53.27	2.040	4.039 ± 0.048	0.79 ± 0.19	172 ± 22	21.2 ± 6.0	$0.294 \pm 0.092 (0.085)$
Tac 18	61.72	2.027	3.931 ± 0.047	1.15 ± 0.23	167 ± 21	30.0 ± 7.1	$0.44 \pm 0.13 (0.11)$
Blank 01	-	2.002	116.4 ± 1.5	0.23 ± 0.16	-	-	-

469

470 Table 4. Analytical ^{36}Cl data and resulting ^{36}Cl CRE ages for samples from Tacaná Volcanic
471 Complex. Age uncertainties (1σ) include production rate errors as well as analytical errors; numbers
472 in parenthesis correspond to analytical errors only.

473

474

475

476 Figure 6 and Table 4 (also supplement material) present the nine ^{36}Cl CRE ages calculated
477 from the samples collected at the summit lava domes “East”, “Northwest” and “Southwest”
478 of Tacaná volcano. On the “East” dome, samples Tac-1, -2 and -3 lead to ^{36}Cl CRE ages of
479 9.7 ± 1.4 ka, 7.3 ± 1.0 ka, 11.0 ± 1.8 ka, respectively. Considering their associated
480 uncertainties, they are statistically indistinguishable and lead to an arithmetic mean ^{36}Cl
481 CRE age and standard deviation of 9.3 ± 1.9 ka. On the “Northwest” dome, the calculated
482 ^{36}Cl CRE ages of 9.7 ± 1.0 ka, 8.0 ± 1.1 ka and 8.9 ± 1.0 (samples Tac-4, -5 and -6) lead to
483 an arithmetic mean ^{36}Cl CRE age of 8.9 ± 0.9 ka, whereas on the “Southwest” dome, the
484 calculated ^{36}Cl CRE ages of 9.8 ± 1.3 ka, 6.7 ± 1.0 ka and 9.4 ± 1.3 ka (samples Tac-7, -8,
485 and -9) lead to an arithmetic mean ^{36}Cl CRE age of 8.6 ± 1.7 ka. Dendrochronological data
486 around the summit area lead to tree ages ranging from 83 to 164 years. The youngest trees
487 are located on the summit of Tacaná dome (83 years, A1, *Juniperus monticola*) at 4058 m
488 a. s. l. A similar age (<100 years) from the thali of *Rhizocarpon geographicum* is obtained.

489 **4.2.2. Horseshoe-shaped crater of Tacaná volcano**

490
491 Remnant lavas from the horseshoe-shaped crater of Tacaná are distributed to the south, east
492 and southeast of the main Tacaná edifice (Figs. 2 and 6). As mentioned before, the 600 m
493 wide crater breached to the NW was produced by the 15 ± 5 ka collapse. Samples from
494 these lavas, which were analyzed in this work, have an andesitic composition (60 wt.%
495 SiO_2) with 6 wt.% alkalis (Fig. 5a). Furthermore, the three samples for ^{36}Cl CRE dating
496 from the southern edge of the horseshoe-shaped crater (samples Tac-10, -11 and -12) lead
497 to ^{36}Cl CRE ages of 5.3 ± 0.6 ka, 0.7 ± 0.2 ka and 7.0 ± 0.8 ka, respectively (Fig. 6, Table 4
498 and supplement material).

499 **4.2.3. “Andesitic lava”**

500
501
502 The “Andesitic lava” was vented at the base of the “Southwest” dome of Tacaná and at the
503 large NE-SW horseshoe-shaped crater (Figs. 2 and 6). Three samples from these lavas that
504 hosted basaltic andesite mafic enclaves were collected. The geochemical analysis of pure
505 lava samples have an andesitic composition varying from 59 to 62 wt.% SiO_2 , although one
506 sample lies at the limit between andesite and dacite compositions (63 wt.% SiO_2 , on

507 anhydrous basis) (Fig. 5a; Table 2). The lava composition is similar to that from the
508 “Southwest” dome and periphery lavas (Fig. 5b-g) and the sampled mafic enclaves are
509 similar to other enclaves reported in previous works (Mora et al., 2004; 2013). Besides, the
510 three ^{36}Cl CRE ages from these “Andesitic” lava samples Tac 16, 17, 18 are 0.5 ± 0.1 ka,
511 0.3 ± 0.1 ka and 0.4 ± 0.1 ka, respectively (Fig 6, Table 4 and supplement material).
512 Considering their associated uncertainties, they are statistically indistinguishable and lead
513 to a mean ^{36}Cl CRE age of 0.4 ± 0.1 ka. Furthermore, lichenometry lead to a minimum age
514 of 390 years (Fig. 7).

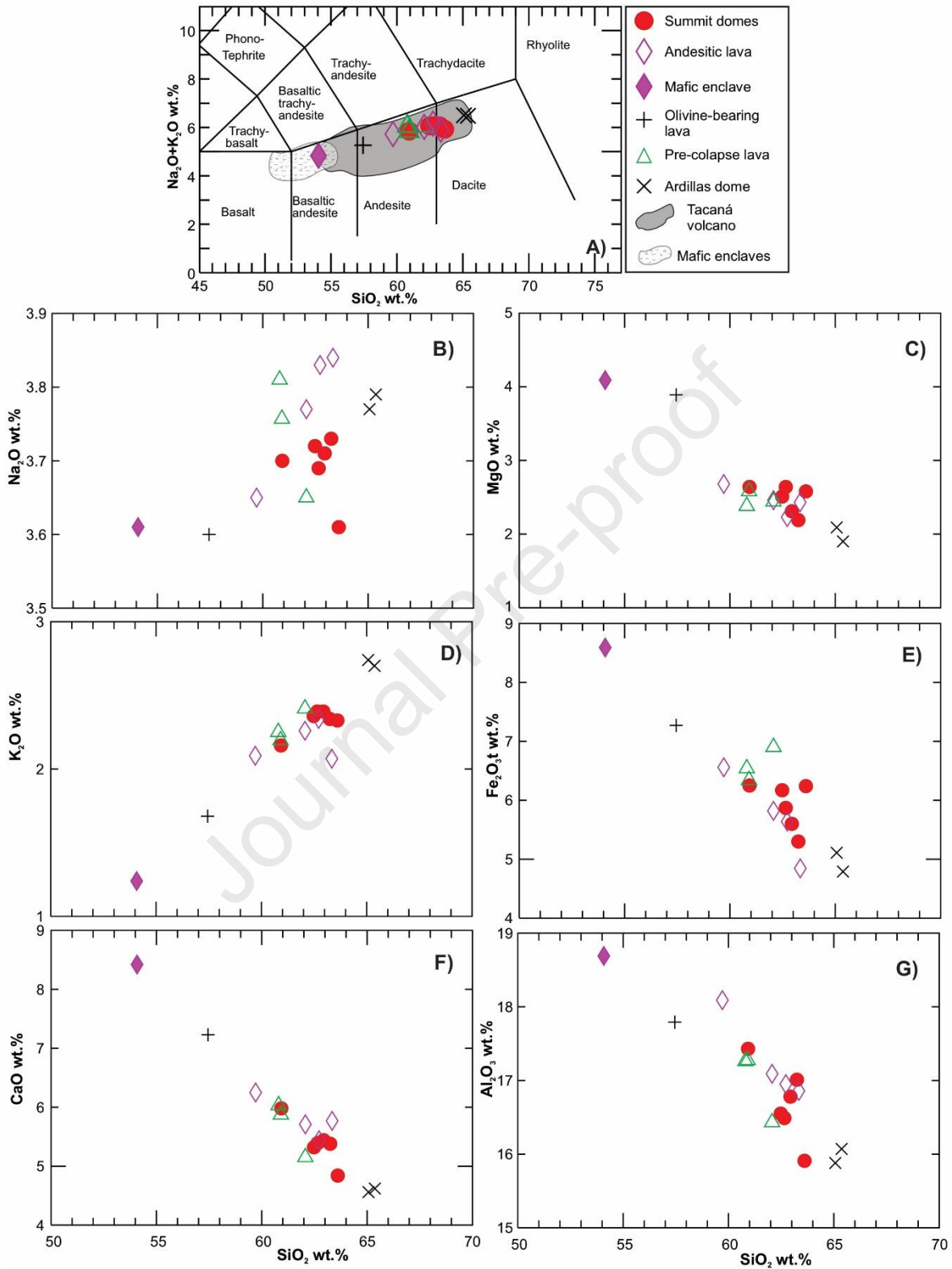
515

516 **4.2.4. Las Ardillas dome**

517 The chemical analyses of two samples from the Ardillas dome (Table 2) complemented
518 with one sample from a previous work (García-Palomo et al., 2006) indicate that the
519 Ardillas dome is the most silicic structure of the TVC. It is dacitic in composition (Fig. 5a)
520 with silica contents of 63-65 wt.% and alkalis of 5.8-6.5 wt.%. All the samples have the
521 lowest values in MgO, CaO, Fe_2O_3 , and Al_2O_3 (Fig. 5b-g), according to their more evolved
522 character (more silica rich). Figure 6 and Table 4 (also supplement material) present the
523 ^{36}Cl CRE ages of the Ardillas lava dome, which are 0.3 ± 0.1 ka and 0.2 ± 0.1 ka (Tac-13
524 and -15) and lead to a mean ^{36}Cl CRE age of 0.3 ± 0.1 ka. Due to the number of ^{36}Cl atoms
525 determined by AMS for sample Tac 14 being similar to that determined for the chemically
526 processed blank considering their associated analytical uncertainties, it is not possible to
527 calculate an exposure age for this sample. However, its ^{36}Cl concentration close to the
528 chemical blank value indicates a very short exposure duration. On top of the Ardillas dome,
529 the tree ages range from 117 to 164 years, whereas trees closer to the eastern vertical wall
530 of the dome have ages ranging from 117 to 138 years (supplement material). In addition,
531 lichenometry provides a minimum age of 300 years (Fig. 7).

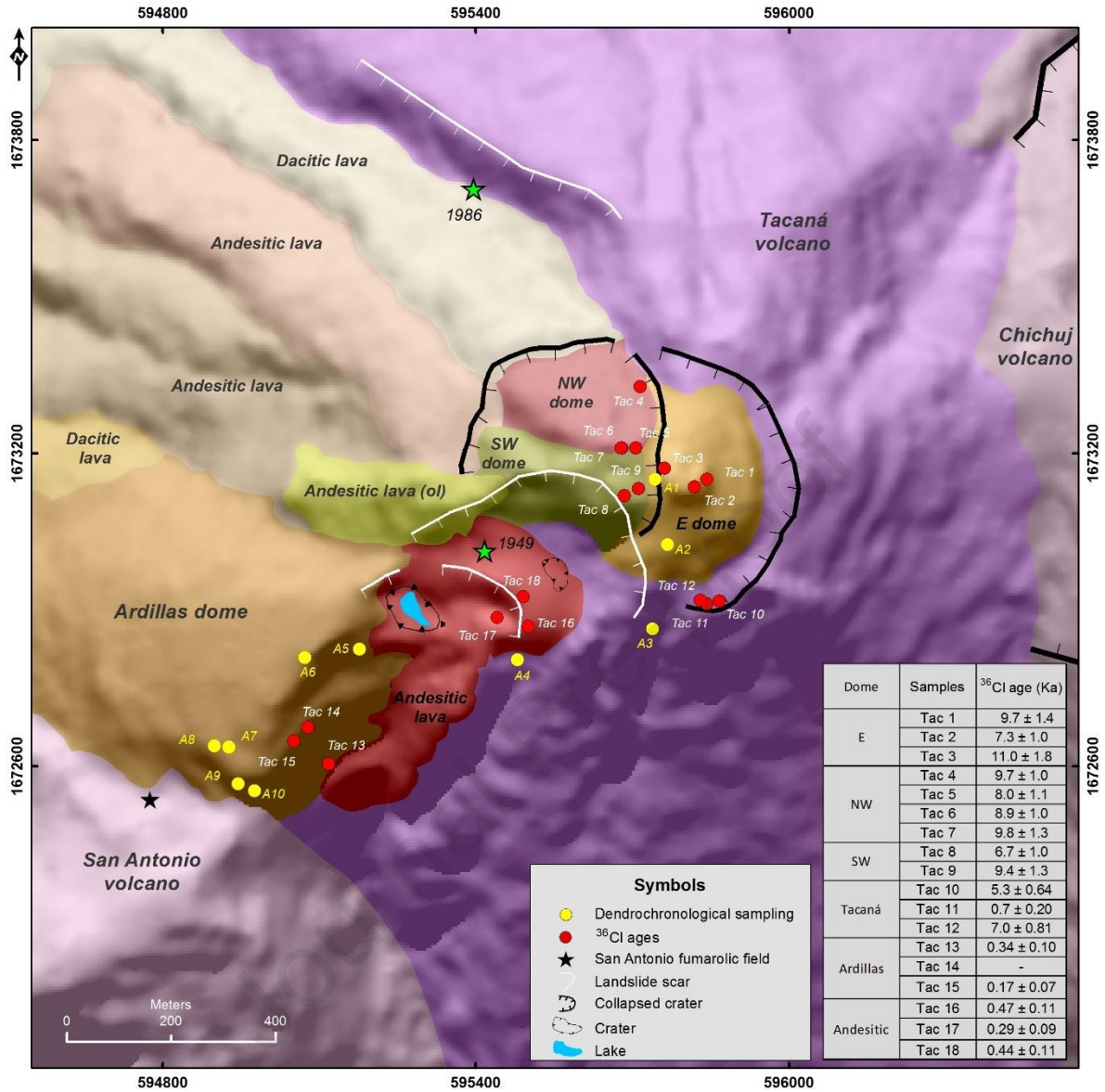
532

533



534

535 Figure 5. Whole-rock chemical composition of Tacaná samples. A) Total alkalis vs silica diagram
 536 (Le Bas et al., 1986) and B-G) binary diagrams. All samples were plotted on anhydrous basis. Gray
 537 and dotted areas were taken from previous works (Mora et al., 2004; Arce et al., 2015).



538

539 Figure 6. Geological map of Tacaná Volcanic Complex. The red spots indicate the location of the
 540 samples collected for ³⁶Cl CRE dating.

541

542

543

544

545

546

547

548



549

550 Figure 7. Detailed photographs of *Rhizocarpon geographicum*. A) A colony formed by several
 551 individuals whom oldest specimen is 390 years, growing on the surface of the “Andesitic lava”; B)
 552 The biggest specimen of *Rhizocarpon geographicum* found at the Ardillas dome yield a minimum
 553 age of 300 years.

554

555 5. Discussion

556

557 5.1. Interpretation of the ^{36}Cl CRE, lichenometry and dendrochronological ages

558 In this study, ^{36}Cl CRE dating was used to determine the age of four lava domes, one
 559 horseshoe-shaped crater and one lava from the summit and the upper part of TVC. Based
 560 on the geomorphology and field observations, the oldest rocks of the TVC summit seem to
 561 be the lavas cut by the collapse scar, followed by lavas that filled the horseshoe-shaped
 562 crater ending with extrusion of the summit domes (Figs. 2 and 6). The ^{36}Cl CRE ages
 563 obtained from the three summit lava domes are statistically indistinguishable considering
 564 their associated uncertainties and provide evidence of an important effusive episode at
 565 around 9 ka. These ages are in good agreement with the explosive Once de Abril eruption
 566 that occurred ca.10 ka (^{14}C age) and dispersed a succession of dense and dilute PDCs
 567 (Macías et al., 2015). Also at ca. 10 ka (Limón-Hernández, 2011), another debris
 568 avalanche, called Tuimanj, occurred towards the north associated with a smaller collapse on
 569 the northern part of the Tacaná scar crater (at Tuimanj hamlet). Hence, Once de Abril

570 eruption and Tuimanj debris avalanche were followed by a voluminous effusive cycle that
571 emplaced the three summit lava domes.

572 Based on the morphology and erosion of the Tacaná summit, it can be deduced that the first
573 dome extruded inside the horseshoe-shaped crater was the “East” dome (radio antenna) at
574 9.3 ± 1.9 ka. It is quite likely that during its growing stage, parts of the dome collapse to the
575 west producing a N-S scar. This is a common feature in growing domes in which unstable
576 parts fail due to the action of the gravity (e.g. Colima volcano, Saucedo et al., 2004).
577 Afterwards, a new batch of andesitic magma emplaced to the west of this N-S scar erecting
578 first the “Northwest” (8.9 ± 0.9 ka) and shortly after the “Southwest” (8.6 ± 1.7 ka)
579 andesitic domes. The tree ages around the summit area range from 83 to 164 years, being in
580 good agreement with that of <100 years inferred from the thali of *Rhizocarpon*
581 *geographicum*. Obviously, these two ages are not related to the emplacement of the summit
582 domes (“East”, “Northwest”, and “Southwest”), but indicate growth recovery after the 1902
583 eruption of Santa Maria volcano that covered the summit of Tacaná with at least 15 cm of
584 ash. This eruption produced a tree-ring growth suppression event in the *Pinus hartwegii*
585 recorded from 1903 to 1908 (Carlón et al., 2020). Therefore, the ^{36}Cl CRE results document
586 that intense effusive activity filled the summit of Tacaná during the Early Holocene.

587 By contrast, the ^{36}Cl CRE ages of ca. 5-7 ka for the lava forming the southern edge of the
588 horseshoe-shaped crater are around 9 ka younger than the associated debris avalanche
589 deposit according to its $^{40}\text{Ar}/^{39}\text{Ar}$ age of 15 ± 5 ka (Macías et al., 2010). Further, they are
590 not consistent with the ^{36}Cl CRE ages of the summit domes (ca. 9 ka), which are
591 stratigraphically younger than the horseshoe-shaped crater and chemically
592 undistinguishable from the samples of the domes (Fig. 5b-g). We therefore infer an
593 underestimation of the ^{36}Cl CRE ages of the horseshoe-shaped crater and hypothesize that
594 gravitational processes affected the limit of the steep cliff of the horseshoe-shaped crater
595 from where the samples were collected. This implies that the sampled surfaces were
596 exposed several thousand years after the collapse event. Therefore, we assume that the ^{36}Cl
597 CRE ages should be considered as minimum ages of the volcanic collapse.

598 As the Ardillas lava dome is older than 760 ± 30 yr BP (Macías et al., 2018), we suspect
599 that the ^{36}Cl CRE dates (0.3 ± 0.1 ka) underestimate the age of the emplacement of this
600 dome. The sampled sites at this structure were to the right of the tensional fractures and
601 very close to an unstable vertical cliff (Fig. 2 and supplement material) to the east sector of
602 the dome. There is evidence of landslides associated probably with the stress regime
603 enhanced by seismicity (Servicio Sismológico Nacional, UNAM;
604 <http://www.ssn.unam.mx>) and heavy rainfalls with an annual precipitation between 4,500
605 and 5,000 mm (<http://www.tapachula.gob.mx>). Thus, we assume that we dated the
606 approximate age of a landslide and not the age of the dome extrusion. Dendrochronology
607 and lichenometry confirm the ^{36}Cl CRE dates with trees ranging between 117 and 164 years
608 and lichen ages of 300 years, respectively. These results show that *in situ*-produced
609 cosmogenic nuclide dating is useful to provide chronological constraints on active mass
610 wasting processes in volcanic environments. Such a scenario further suggests that a
611 monitoring studio (cameras, seismic stations) of these steep cliffs of the Ardillas dome
612 might be necessary to alert downstream populations of future landslides.

613 A young ^{36}Cl CRE age (0.4 ± 0.1 ka) has also been obtained from the “Andesitic lava”.
614 Here, samples were collected from the west margin of the lava, which seems to be affected
615 by a small landslide that exhibits a crater-like morphology opened to the west (Fig. 6 and
616 supplement material; samples Tac 16-18). Chronological data from lichenometry (390
617 years) also support the ^{36}Cl CRE age, demonstrating a consistent young exposure of the
618 sampled area. Given the observations of instability, we suggest that the ^{36}Cl CRE and
619 lichenometry ages represent the age of a historical collapse likely associated with the
620 phreatic explosion crater present at the base of the large NE-SW landslide that dispersed
621 breccia and pyroclastic deposits atop the lava flow. In this sense, more research must be
622 carried out to determine the exact age of the eruption not reported yet.

623 **5.2. Refined Holocene volcanic history of TVC and hazards implications**

624

625 After the ca.15 ka collapse of Tacaná that left a horseshoe-shaped crater, renewed activity
626 ensued andesitic lavas (e.g. ca.12 ka Agua Zarca) that partially filled the collapse
627 depression and crater. At around 10 ka, the largest explosive Holocene event of Tacaná

628 took place with the generation of PDCs that were dispersed radially around the volcano
629 affecting up to the base of the cone (Macías et al 2010). This eruption was produced during
630 open vent conditions (no domes involved atop), ejecting a low altitude eruptive column that
631 was called the Once de Abril ash flow sequence (Macías et al., 2015). At about the same
632 time, another collapse generated the Tuimanj debris avalanche to the north (Limón-
633 Hernández, 2011) that was smaller than the Agua Caliente debris avalanche. After these
634 volcanic events, Tacaná experienced effusive activity with the emplacement of the “East”
635 lava dome at 9.3 ± 1.9 ka, followed by the extrusion of the “Southwest” and “Northwest”
636 lava domes at 8.6 ± 1.7 ka and 8.9 ± 0.9 ka (Fig. 6) that filled the horseshoe-crater as we
637 know it today.

638

639 Then, explosive activity took place around the summit of the TVC with at least nine small
640 eruptions: (i) Papales ash flow deposit 1 (8683-8180 cal yr BP) (Macías et al., 2015); (ii)
641 the Chocab pumice flow with charcoal embedded at 7933-7595 cal yr BP (García-Palomo
642 et al., 2006); (iii) a pyroclastic sequence of flows and surges dated at 6998-6400 cal yr BP;
643 (iv) a pyroclastic surge sequence with an underlying paleosol dated at 2920-2715 cal yr BP,
644 (v) a scoria block and ash flow with charcoal dated at 924-748 cal yr BP; and (vi), the
645 phreatomagmatic eruption followed by a sub-Plinian column that dispersed a pumice-rich
646 fallout some 935-748 cal yr BP (Macías et al., 2018), forming an elongated crater lake of
647 80 x 60 m in diameter (Fig. 2). We also report a minimum ^{36}Cl CRE age of the “Andesitic
648 lava” of 0.4 ± 0.1 ka that was emitted somewhere close to the Southwest dome. This age is
649 supported by chronological data from lichenometry (390 years). The “Andesitic lava” was
650 disrupted by an elongated explosion crater (60 x 25 m) made of breccia and pyroclastic
651 deposits dispersed on the lava flow. Based on its different composition, it is likely that the
652 “Andesitic lava” was emitted before the “Northwest” and “Southwest” domes. The olivine-
653 bearing lava and the dome samples display negative trends in MgO, Fe₂O₃, CaO, and Al₂O₃
654 (Fig. 5b-g), suggesting their magmatic link and fractional crystallization of mafic phases at
655 depth (350 MPa; Mora et al., 2013). Besides, magma mixing between mafic melts and
656 andesitic magmas hosted in the reservoir can produce mafic enclaves (Coombs et al., 2003;
657 Mora et al., 2013); such mixing mechanism is commonly considered as a trigger of
658 volcanic eruptions (Manrique et al., 2020). Furthermore, the young ^{36}Cl CRE dates

659 determined for the Ardillas lava dome (0.2 ± 0.1 ka) and the “Andesitic lava” flow ($0.4 \pm$
660 0.1 ka) testify the occurrence of active gravitational processes. These processes are related
661 to a NE-SW fissure along which occur tensional fractures, landslide scars, vents of
662 phreatomagmatic and phreatic explosions (e.g. 1986 explosion), hydrothermal fluids, and
663 fumaroles.

664 Three more historical explosive eruptions have been recognized on the slopes of Tacaná
665 volcano. One of them produced a yellow pyroclastic flow deposit dated at 536-157 cal yr
666 BP (Limón-Hernández, 2011). Another one produced an ash flow deposit called the Papales
667 ash flow dated at 496 - To Present cal yr BP (Macías et al., 2015), whereas a white
668 pyroclastic surge deposit was dated at 285 - To Present cal yr BP (Macías et al., 2015). The
669 last events at Tacaná were small explosions that took place during the last two centuries in
670 1855-1856 (Mercado and Rose, 1992; Carlón et al., 2020), 1949 (Müllerried 1951), and
671 1986 (De la Cruz-Reyna et al., 1989).

672 The presence of lava domes (ca. 9 ka) at the Tacaná summit (together with the lava
673 emplaced to the north) infilling the horseshoe-shaped crater suggests that after the ca.15 ka
674 sector collapse (Agua caliente debris avalanche), the activity shifted from explosive to
675 effusive eruptions, lasting for centuries or thousands of years. This is a common
676 phenomenon observed in many volcanoes after a sector collapse (e.g. Popocatépetl, Siebe
677 et al., 2017) probably related to degassing of magma. Furthermore, lava domes represent
678 the location of volcanic conduits from which magma was ejected to the surface. Thus, the
679 summit lava domes of Tacaná volcano emplaced during Early Holocene blocked the
680 volcanic conduit because no other craters are exposed at the summit today. Therefore, the
681 question arises where the vent responsible for the Late to Middle Holocene explosive
682 eruptions is located. A blockage of the conduit in the meantime could prevent the degassing
683 of the magma reservoir producing overpressure and eventually explosive eruptions when
684 the internal pressure reaches the rupture pressure of the surface. This could have produced
685 the nine dated explosive eruptions at the TVC (Macías et al., 2015). The magma
686 accumulated in the reservoir sought other paths to get to the surface as the set of NE-SW
687 fractures observed nowadays (Fig. 4) from which the phreatomagmatic explosion formed a
688 crater-lake around 0.76 ka (Macías et al., 2015), that was drained during the historic

689 phreatic explosion of 1949. The study of lava domes has important implications to specify
690 the behavior of eruption style (explosive-effusive) and the generation of block-and-ash
691 flows (i.e.: Colima volcano; Saucedo et al., 2002) that are one of the most dangerous
692 phenomena in explosive events (Vázquez et al., 2019). Explosive eruptions like those dated
693 at 5 and 2 ka (Macías et al., 2015) could be related to the gravitational collapse of the
694 external parts of summit domes and/or lava fronts (Saucedo et al., 2019).

695 We have recognized two NE-SW and two NW-SE scar collapses around the TVC summit.
696 These scar collapses have orientations in agreement with the present stress regime in the
697 area. Geometrically, this suggests that the location and evolution of the TVC could be
698 related to fractures with a $N65^{\circ}$ E to $N75^{\circ}$ E direction, which are in good agreement with
699 the results of García-Palomo et al. (2006), and could be associated with a large-scale
700 fracture with the same orientation (Fig. 4). Such stress regime and fault system is typical of
701 an active transtensive tectonic environment. Because no primary volcanic deposits are
702 associated with these events (i.e. debris avalanche deposits, or fallout and pyroclastic flow
703 deposits), they likely were produced by gravitational collapses only. The Tacaná summit
704 domes are highly viscous based on their acidic andesitic to dacitic compositions with
705 pronounced steep edges representing unstable parts prone to collapse. In addition, current
706 Google Earth images show active landslides taking place in the eastern portion of Ardillas
707 dome and the northeastern part of San Antonio volcano. This area is affected by the NE-
708 SW tension fractures displayed in figure 4, which past landslides dated in this study
709 (“Andesitic lava” and Ardillas dome) area associated with it. Therefore, this persistent
710 volcanic activity and mass waste processes highlight the need for a permanent monitoring
711 system of the complex, which would be essential to predict future geologic hazards and
712 mitigate the associated risks for the nearby populations.

713 A better constraint of the eruptive chronology of the Holocene activity of the TVC has been
714 complemented with our results highlighting an intense effusive volcanic and landslide
715 activity during the Holocene. This Holocene volcanic activity of the TVC is similar to other
716 volcanoes in Mexico as Colima and Popocatepetl. Colima volcano (the most active volcano
717 in Mexico) has experienced at least nine explosive eruptions intercalated with dome-
718 forming events (Macías and Arce, 2019), and several small-magnitude eruptions (1991,

719 2000, 2002, 2006, 2015) (Rodríguez-Elizarrarás et al., 1991; Saucedo et al., 2005, 2010;
720 Mora et al., 2004; Capra et al., 2016). Popocatépetl volcano has recorded 12 explosive
721 eruptions during the Holocene (Macías and Arce, 2019), involving three large magnitude
722 Plinian eruptions (Siebe et al., 1995; Siebe and Macías, 2006). Therefore, the TVC stands
723 among the most active (hazardous) volcanoes in Mexico during the Holocene. In terms of
724 risk, however, the TVC is the second most dangerous volcano just after Popocatépetl,
725 because a future eruption would threaten more than around 300,000 people, including the
726 city of Tapachula. A Plinian eruption would disrupt life in Central America affecting main
727 cities of Belize, Guatemala, El Salvador, Honduras, and Mexico (Vázquez et al., 2019).

728 **6. Conclusions**

729 ^{36}Cl CRE dating, dendrochronology and lichenometry were combined to determine the
730 unknown ages of lava domes, a steep cliff of the late Pleistocene horseshoe-shaped crater,
731 and one lava from Tacaná volcano. The summit lava domes (“East”, “Northwest” and
732 “Southwest”) are dated consistently at 9.3 ± 1.9 ka; 8.9 ± 0.9 ka; 8.6 ± 1.7 ka, providing
733 evidence of a voluminous effusive activity around 9 ka that followed a major explosive
734 eruption of Tacaná (Once de Abril ash flow sequence).

735

736 Furthermore, ^{36}Cl CRE ages of the cliff of the horseshoe-shaped crater of ca. 5-7 ka most
737 likely correspond to gravitational rock fall events rather than to the collapse event of the
738 crater, which is expected to predate the summit domes according to the volcanic
739 stratigraphy. Strikingly, the combination of ^{36}Cl CRE ages, lichenometry and
740 dendrochronology in the “Andesitic lava” and Ardillas dome resulted also useful to detect
741 active processes associated with NE-SW landslide scars, explosion craters, phreatic vents,
742 fumarole activity, and tensional fractures all of which are perpendicular to the NW-SE
743 minimum stress regime (σ_3) in the area. Therefore, we conclude that Tacaná is one of the
744 most active volcanoes in Mexico, probably the third just after the Colima and Popocatépetl
745 volcanoes. This scenario implies the need for a significant effort to mitigate volcanic
746 hazards and associated risks (i. e. volcanic collapses) that can affect the nearby populations.

747 **Acknowledgements**

748 This research was supported by Consejo Nacional de Ciencia y Tecnología (CONACyT)
749 projects A1-S-21156 to J. Alcalá Reygosa and PN522 to J.L. Macías. Dirección de Asuntos
750 del Personal Académico (DGAPA-PAPIIT) IN112720 to J.L. Macías, and IN101620 to J.L.
751 Arce. The ^{36}Cl measurements were performed at the ASTER AMS national facility
752 (CEREGE, Aix en Provence) which is supported by the INSU/CNRS, the ANR through the
753 "Projets thématiques d'excellence" program for the "Equipements d'excellence" ASTER-
754 CEREGE action and IRD. We are also grateful to Irma Fabiola Mendiola López and Omar
755 López Arevalo (Instituto de Geofísica Unidad Morelia; Universidad Nacional Autónoma de
756 México) whom helped in the physical treatment of the ^{36}Cl samples. We are indebted with
757 J.I. Lara, A. Lugo, M. Mendoza, G. Sosa for sharing field campaigns with us at the
758 volcano. We are grateful for the constructive comments by Naki Akcar and Venera R. May
759 whom greatly improved the manuscript.

760 **References**

761 Alcalá-Reygosa, J., Palacios, D., Schimmelpfennig, I., Vázquez-Selem, L., García-Sancho,
762 L., Franco-Ramos, O., Villanueva, J., Zamorano, J. J., Aster Team (Aumaitre, G., Boulès,
763 D., Keddadouche, K.) 2018a. Dating late Holocene lava flows in Pico de Orizaba (Mexico)
764 by means of in situ-produced cosmogenic ^{36}Cl , lichenometry and dendrochronology.
765 *Quaternary Geochronology* 47, 93-106. <https://doi.org/10.1016/j.quageo.2018.05.011>.

766 Alcalá-Reygosa, J., Arce, J. L., Schimmelpfennig, I., Salinas, E. M., Rodríguez, M. C.,
767 Léanni, L., Aster Team (Aumaitre, G., Boulès, D., Keddadouche, K.) 2018b. Revisiting
768 the age of the Jumento volcano, Chichinautzin Volcanic Field (Central Mexico), using in
769 situ-produced cosmogenic ^{10}Be . *Journal of Volcanology and Geothermal Research* 366,
770 112-119. <https://doi.org/10.1016/j.jvolgeores.2018.10.005>.

771 Arce, J.L., Macías, J.L., Vázquez-Selem, L. 2003. The 10.5 ka Plinian eruption of Nevado
772 de Toluca, Mexico: stratigraphy and hazard implications. *Geological Society of America*
773 *Bulletin* 115, 230-248.

774 Arce, J.L., Macías, J.L., Gardner, J.E., Rangel, E., 2012. Reconstruction of the Sibinal
775 Pumice, an andesitic Plinian eruption at Tacaná Volcanic Complex, Mexico-Guatemala.
776 *Journal of Volcanology and Geothermal Research* 217-218, 39-55.
777 <https://doi.org/10.1016/j.jvolgeores.2011.12.013>.

778

- 779 Arce, J.L., Walker, J., Keppie, J. D., 2015. Petrology and geochemistry of El Chichón and
780 Tacaná: two active, yet contrasting Mexican volcanoes. In: Active Volcanoes of Chiapas
781 (Mexico): El Chichón and Tacaná. Edited by T. Scolamacchia and J.L. Macías. Springer-
782 Verlag, 25-43 p. https://doi:10.1007/978-3-642-25890-9_2.
- 783 Arnold, M., Aumaître, G., Boulès, D. L., Keddadouche, K., Braucher, R., Finkel, R. C.,
784 Nottoli, E., Benedetti, L., Merchel, S. 2013. The French accelerator mass spectrometry
785 facility ASTER after 4 years: status and recent developments on ^{36}Cl and ^{129}I . Nuclear
786 Instruments and Methods in Physical Research 294, 24-28.
787 <https://doi.org/10.1016/j.nimb.2012.01.049>.
- 788 Capra, L., Macías J.L., Cortés, A., Davila, N., Saucedo, R., Osorio-Ocampo, S., Arce, J.L.,
789 Gavilanes-Ruíz, J.C., Corona-Chávez, P., García-Sánchez, L., Sosa-Ceballos, G., Vázquez,
790 R. 2016. Preliminary report on the July 10-11, 2015 eruption at Volcán de Colima:
791 Pyroclastic density currents with exceptional runouts and volumes. Journal of
792 Volcanology and Geothermal Research 310, 39-49.
793 <https://doi.org/10.1016/j.jvolgeores.2015.11.022>.
- 794
- 795 Carlon, T., Macías, J.L., Mendoza, M., and Villanueva, J. 2020. Evidence of volcanic
796 activity in the growth rings of trees in the Tacaná Volcano, Mexico-Guatemala. Journal of
797 Canadian Forest 50: 65-72. <http://doi.org/10.1139/cjfr-2019-0214>.
- 798
- 799 Coombs, M. L., Eichelberger, J. C., Rutherford, M. J. 2003. Experimental and textural
800 constraints on mafic enclave formation in volcanic rocks. Journal of Volcanology and
801 Geothermal Research 119, 125-144. [https://doi.org/10.1016/S0377-0273\(02\)00309-8](https://doi.org/10.1016/S0377-0273(02)00309-8).
- 802
- 803 De la Cruz-Reyna, S., Armienta, M.A., Zamora, V., Juárez, F. 1989. Chemical changes in
804 spring waters at Tacaná Volcano, Chiapas, México. Journal of Volcanology and
805 Geothermal Research 38, 345-353. [https://doi.org/10.1016/0377-0273\(89\)90047-4](https://doi.org/10.1016/0377-0273(89)90047-4).
- 806
- 807 Dunai, T.J., 2010. Cosmogenic nuclides. Principles, Concepts and Applications in the
808 Earth Surface Sciences. Cambridge University Press, pp. 198.
- 809
- 808 Espíndola, J. M., Medina, F. M., and De los Ríos, M., 1989. A C-14 age determination in
809 the Tacaná volcano (Chiapas, Mexico). Geofísica Internacional 28, 123-128.
- 810
- 811 Fink, D., Vogt, S., Hotchkis, M. 2000. Cross-sections for ^{36}Cl from Ti at $E_p = 35\text{--}150$
812 MeV: applications to *in-situ* exposure dating. Nuclear Instruments and Methods in Physical
813 Research Section B Beam Interaction Mater and Atoms 172, 861-866.
814 [https://doi.org/10.1016/S0168-583X\(00\)00200-7](https://doi.org/10.1016/S0168-583X(00)00200-7).

- 815 García-Palomo, A., Macías, J.L., Arce, J.L., Mora, J.C., Hughes, S., Saucedo, R.,
816 Espíndola, J.M., Escobar, R., Layer, P. 2006. Geological evolution of the Tacaná Volcanic
817 Complex, México-Guatemala. In: Rose WI, Bluth GJS, Carr MJ, Ewert JW, Patino LC,
818 Vallance JW (eds) Natural Hazards in Central America. Boulder, Colorado. Geological
819 Society of America, Special Paper 412, 39-57. [https://doi.org/10.1130/2006.2412\(03\)](https://doi.org/10.1130/2006.2412(03)).
820
- 821 Garduño, V.H., Macías, J.L., Molina, R. 2015. Geodynamic setting and pre-volcanic
822 geology of active volcanism in Chiapas. In: Active Volcanoes of Chiapas (México): El
823 Chichón and Tacaná. Edited by T. Scolamacchia and J.L. Macías. Springer Verlag, 1-
824 24. DOI 10.1007/978-3-642-25890-9_1.
- 825 Jomelli, V., Lane, T., Favier, V., Masson-Delmotte, V., Swingedouw, D., Rinterknecht, V.,
826 Schimmelpfennig, I., Brunstein, D., Verfaillie, D., Adamson, K., Leanni, L., Mokadem, F.,
827 Aumaitre, G., Bourles, D.L., Keddadouche, K. 2016. Paradoxical cold conditions during
828 the medieval climate anomaly in the Western Arctic. *Scientific Reports* 6, 32984.
829 <http://dx.doi.org/10.1038/srep32984>.
- 830 Limón-Hernández, C. G. 2011. Estratigrafía y morfología de los flujos de lava y depósitos
831 asociados a la actividad efusiva del volcán Tacaná, México-Guatemala. Master thesis,
832 Posgrado en Ciencias de la Tierra UNAM, México, 125 p.
833
- 834 Macías J. L., Espíndola J. M., García-Palomo A., Scott K. M., Hughes S., Mora J. C.
835 2000. Late Holocene Peléan style eruption at Tacaná Volcano,
836 Mexico-Guatemala: Past, present, and future hazards. *Bulleting Geological Society of*
837 *America* 112, 1234-1249.
838 [https://doi.org/10.1130/00167606\(2000\)112<1234:LHPEAT>2.0.CO;2](https://doi.org/10.1130/00167606(2000)112<1234:LHPEAT>2.0.CO;2)
839
- 840 Macías, J.L., Arce, J.L., García-Palomo, A., Mora, J.C., Layer, P.W., Espíndola, J.M. 2010.
841 Late-Pleistocene flank collapse triggered by dome growth at Tacaná Volcano, México-
842 Guatemala, and its relationship to the regional stress regime. *Bulletin of Volcanology* 72,
843 33-53.
844
- 845 Macías, J.L., Arce, J.L., Layer, P.W., Saucedo, R., Mora, J.C. 2015. Eruptive history of the
846 Tacaná Volcanic Complex. In: Scholamacchia T, Macías JL (Eds.) *Active Volcanoes of*
847 *Chiapas (Mexico) El Chichón and Tacaná, Active Volcanoes of the world*, Springer Verlag
848 pp. 115-138.
849
- 850 Macías, J.L., Arce, J.L., Capra, L., Saucedo, R., Sánchez-Núñez, J.M. 2018. Late Formative
851 flooding of Izapa after an eruption of Tacaná volcano. *Ancient Mesoamerica* 29:361-371.
852

- 853 Macías, J. L., Arce, J. L. 2019. Volcanic Activity in Mexico During the Holocene. In *The*
854 *Holocene and Anthropocene Environmental History of Mexico* (pp. 129-170). Springer,
855 Cham. https://doi.org/10.1007/978-3-030-31719-5_8.
- 856 Manrique, N., Samaniego, P., Médard, E., Schiavi, F., Mariño, J., Liorzou, C. 2020. Pre-
857 eruptive magmatic processes associated with the historical (218 ± 14 aBP) explosive
858 eruption of Tutupaca volcano (southern Peru). *Bulletin of Volcanology*, 82:6,
859 <https://doi.org/10.1007/s00445-019-1335-4>.
- 860 Marrero, S. M., Phillips, F. M., Caffee, M. W., Gosse, J. C., 2016. CRONUS-Earth
861 cosmogenic ^{36}Cl calibration. *Quaternary Geochronology* 31, 199-219.
862 <https://doi.org/10.1016/j.quageo.2015.10.002>.
- 863 Martíni, M., Capaccioni, B., Giannini, L., 1987. Ripresa dell'attività sismica e fumarolica al
864 Vulcano di Tacaná (Chiapas, Messico) dopo un quarantennio di quiescenza. Estrato da
865 *Bollettino del Gruppo Nazionale per la Vulcanología*, 467-470.
- 866 Mercado, R., Rose, W.I. 1992. Reconocimiento geológico y evaluación preliminar de
867 peligrosidad del Volcán Tacaná, Guatemala/México. *Geofísica Internacional* 31(3): 205-
868 237.
- 869 Merchel, S., Bremser, W., Alfimov, V., Arnold, M., Aumaître, G., Benedetti, L., Bourles,
870 D.L., Caffee, M., Fifield, L.K., Finkel, R.C., Freeman, S.P.H.T., Martschini, M., Matsushi,
871 Y., Rood, D.H., Sasa, K., Steier, P., Takahashi, T., Tamari, M., Tims, S.G., Tosaki, Y.,
872 Wilcken, K.M., Xu, S., 2011. Ultra-trace analysis of ^{36}Cl by accelerator mass
873 spectrometry: an interlaboratory study. *Anal. Bioanal. Chem.*
874 <https://doi.org/10.1007/s00216-011-4979-2>.
- 875 Mora, J.C., Macías, J.L., García-Palomo, A., Espíndola, J.M., Manetti, P., and Vaselli, O.
876 2004. Petrology and geochemistry of the Tacaná Volcanic Complex, Mexico-Guatemala:
877 Evidence for the last 40 000 yr of activity. *Geofísica Internacional* 43, 331-359.
878
- 879 Mora, J. C., Gardner, J. E., Macías, J. L., Meriggi, L. 2013. Magmatic controls on eruption
880 dynamics of the 1950 yr B.P. eruption of San Antonio Volcano, Tacaná Volcanic Complex,
881 Mexico–Guatemala. *Journal of Volcanology and Geothermal Research* 262, 134-
882 152. <https://doi.org/10.1016/j.jvolgeores.2013.06.002>.
- 883
- 884 Müllerried, F.K.G., 1951. La reciente actividad del Volcán Tacaná, Estado de Chiapas, a
885 fines de 1949 y principios de 1950. Informe del Instituto de Geología, UNAM, 28p.
- 886 N.O.A.A, 1976. U.S. Standard Atmosphere. US Gov. Print. Off.

- 887 Palacios, L., García-Sancho, Zamorano, J.J., Andrés, N., Pintado, A., 2012. The
888 deglaciation of Iztaccíhuatl volcano (Mexico) from the Little Ice Age maximum to the
889 present, determined by photogrammetry and lichenometry. *Geophysical Research Abstracts*
890 14, EGU2012–3755 2012.
- 891 Rodríguez-Elizarrarás, S., Siebe, C., Komorowski, J. C., Espíndola, J. M., Saucedo, R.
892 1991. Field observations of pristine block and ash flow deposits emplaced April 16-17
893 1991 at Volcán de Colima, Mexico. *Journal of Volcanology and Geothermal Research* 48
894 (3-4), 399-412. [https://doi.org/10.1016/0377-0273\(91\)90054-4](https://doi.org/10.1016/0377-0273(91)90054-4).
- 895 Rouwet, D., Taran, Y., Inguaggiato, S., Varley, N. 2004. Hydrothermal activity at Tacaná
896 volcano, Mexico–Guatemala. In: Wanty R, Seal R II (eds) WRI-11. Taylor and Francis
897 Group, London, 173–176.
- 898 Rouwet, D., Inguaggiato, S., Taran, Y., Varley, N., Santiago, J.A., 2009. Chemical and
899 isotopic compositions of thermal springs, fumaroles and bubbling gases at Tacaná Volcano
900 (Mexico-Guatemala): implications for volcanic surveillance. *Bulletin of Volcanology* 71,
901 319-335.
- 902 Saucedo, R., Macías, J.L., Bursik, M., Mora, J.C., Gavilanes, J.C., Cortes, A. 2002.
903 Emplacement of pyroclastic flows during the 1998-1999 eruption of Volcán de Colima,
904 Mexico. *Journal of Volcanology and Geothermal Research* 117 (1-2), 129-153.
905 [https://doi.org/10.1016/S0377-0273\(02\)00241-X](https://doi.org/10.1016/S0377-0273(02)00241-X).
- 906 Saucedo, R., Macías, J.L., and Bursik, M.I., 2004. Merapi-type pyroclastic flows produced
907 during the 1991 eruption of Colima Volcano: stratigraphy, sedimentology and emplacement
908 mechanisms. *Bulletin of Volcanology* 66, 291-306.
- 909 Saucedo, R., Macías, J.L., Sheridan, M.F., Bursik, M.I., Komorowski, J.C. 2005. Modeling
910 of pyroclastic flows of Colima Volcano, Mexico: Implications for hazard
911 assessment. *Journal of Volcanology and Geothermal Research* 139, 103-115.
912 <https://doi.org/10.1016/j.jvolgeores.2004.06.019>.
- 913
- 914 Saucedo, R., Gavilanes-Ruiz, J.C., Macías, J.L., Arce, J.L., Komorowski, J.C., Gardner, J.,
915 Valdez-Moreno, G., (2010). Eyewitness, stratigraphy, chemistry, and eruptive dynamics of
916 the 1913 Plinian eruption of Volcán de Colima, México. *Journal of Volcanology and*
917 *Geothermal Research*, 191: 149-166. <https://doi.org/10.1016/j.jvolgeores.2010.01.011>.
- 918 Saucedo, R.1, Macías, J.L., Gavilanes-Ruiz, J.C., Bursik, M.I., and Vargas-Gutiérrez, V.,
919 2019. Pyroclastic density currents at Volcán de Colima. N. Varley et al. (eds.), *Volcán de*

- 920 Colima, Active Volcanoes of the World, https://doi.org/10.1007/978-3-642-25911-1_4,
921 Chapter 12, 111-140 p.
- 922 Schimmelpfennig, I., Benedetti, L., Finkel, R., Pik, R., Blard, P. H., Bourle, D., Burnard,
923 P., Williams, A. 2009. Sources of in-situ ^{36}Cl in basaltic rocks. Implications for cali-
924 bration of production rates. *Quaternary Geochronology* 4, 441-461.
925 <https://doi.org/10.1016/j.quageo.2009.06.003>.
- 926 Schimmelpfennig, I., Benedetti, L., Garreta, V., Pik, R., Blard, P. H., Burnard, P., Bourlès,
927 D., Finkel, R., Ammon, K., Dunai, T. 2011. Calibration of cosmogenic ^{36}Cl production
928 rates from Ca and K spallation in lava flows from Mt. Etna (38°N, Italy) and Payun Matru
929 (36°S, Argentina). *Geochimica et Cosmochimica Acta* 75, 2611-2632.
930 **[10.1016/j.gca.2011.02.013](https://doi.org/10.1016/j.gca.2011.02.013)**.
- 931 Schimmelpfennig I, Schaefer J, Putnam A, Koffman T, Benedetti L, Ivy-Ochs S, ASTER
932 Team, Schlüchter C. 2014. ^{36}Cl production rate from K-spallation in the European Alps
933 (Chironico landslide, Switzerland). *Journal of Quaternary Science* 29, 407-413.
934 <https://doi.org/10.1002/jqs.2720>.
- 935 Siebe, C.G., Macías, J.L., Abrams, M., Elizarraras, R.S., Castro, R., Delgado, H.
936 1995. Quaternary Explosive Volcanism and Pyroclastic Deposits in East-Central Mexico:
937 Implications for Future Hazards. In: Chacko, J.J., and Whitney, J.A., (Eds.), *Guidebook of*
938 *Geological Excursions for the 1995 Annual Meeting of the Geological Society of America*,
939 *New Orleans, Book 1*, p. 1-48.
- 940
941 Siebe, C., Macías, J.L. 2006. Volcanic hazards in the Mexico City metropolitan area from
942 eruptions at Popocatepetl, Nevado de Toluca, and Jocotitlán stratovolcanoes and
943 monogenetic scoria cones in the Sierra de Chichinautzin Volcanic Field. *in* Siebe, C.,
944 Macías, J.L., and Aguirre-Díaz, G.J., eds., *Neogene-Quaternary continental margin*
945 *volcanism: A perspective from Mexico*. Geological Society of America. Special Paper 402,
946 p. 237–252. [doi: 10.1130/2006.2402\(05\)](https://doi.org/10.1130/2006.2402(05)).
- 947 Siebe, C., Salinas, S., Arana-Salinas, L., Macías, J.L., Gardner, J., and Bonasia, R., 2017.
948 The ~23,500 yr ^{14}C BP White Pumice Plinian eruption and associated debris avalanche and
949 Tochimilco lava flow of Popocatepetl volcano, México. *Journal of Volcanology and*
950 *Geothermal Research* 333–334, 66-95. <https://doi.org/10.1016/j.jvolgeores.2017.01.011>.
- 951 Stone, J., 2000. Air pressure and cosmogenic isotope production. *Journal of Geophysical*
952 *Research* 105, 23,753-23,759. <https://doi.org/10.1029/2000JB900181>.

- 953 Stone, J.O., Fifield, K., Vasconcelos, P., 2005. Terrestrial chlorine-36 production from
954 spallation of iron. In: 10th International Conference on Accelerator Mass Spectrometry,
955 Berkeley, USA.
- 956 Stokes, M.A., Smiley, T.L. 1996. An introduction to tree-ring dating. The University of
957 Arizona Press, Tucson, Arizona.
- 958
- 959 Vázquez-Selem, L., Heine, K., 2011. Late quaternary glaciation in Mexico. In: Ehlers, J.,
960 Gibbard, P.L., Hughes, P.D. (Eds.), Quaternary Glaciations - Extent and Chronology. A
961 Closer Look. Elsevier, Amsterdam, pp. 849–861. <http://doi.org/10.1016/B978-0-444-53447-7.00061-1>.
- 962
- 963
- 964 Vázquez, R., Bonasia, R., Folch, A., Arce, J.L., Macías, J.L. 2019. Tephra fallout hazard
965 assessment at Tacaná volcano (Mexico). *Journal of South American Earth Sciences* 91,
966 253-259. <https://doi.org/10.1016/j.jsames.2019.02.013>.
- 967 Vermeesch, P., 2007. CosmoCalc: an excel add-in for cosmogenic nuclide calculations. *G-*
968 *cubed* 8, 1525-2027.
- 969 Ward, G. K., Wilson, S. R. 1978. Procedures for comparing and combining radiocarbon age
970 determinations: a critique. *Archaeometry* 20 (1), 19-31. <https://doi.org/10.1111/j.1475-4754.1978.tb00208.x>.
- 971
- 972
- 973 Williams, S. N., Self, S., 1983. The October 1902 Plinian eruption of Santa Maria volcano,
974 Guatemala. *Journal of Volcanology and Geothermal Research* 16, 33-56.
975 [https://doi.org/10.1016/0377-0273\(83\)90083-5](https://doi.org/10.1016/0377-0273(83)90083-5).
- 976
- 977
- 978
- 979
- 980
- 981
- 982

983

984

985

986

987

988

SUPPLEMENTS

Journal Pre-proof



989

990 Detailed photographs of the samples collected for ^{36}Cl CRE dating from the summit lava domes of
 991 Tacaná volcano.

992

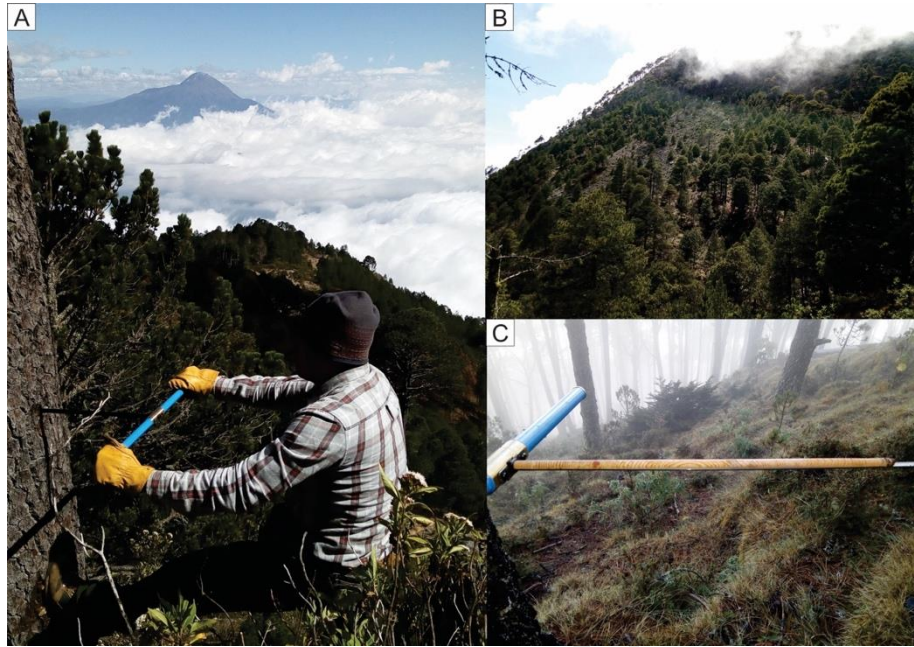
993

994



995

996 Detailed photographs of the samples collected for ^{36}Cl CRE dating from the cliff collapse scar, the
 997 Ardillas dome and the “Andesitic lava” from Tacaná Volcanic Complex.
 998



999

1000 Detailed photographs of the samples collected for dendrochronology. A) Sampling a specimen of
1001 *Pinus hartwegii* Lindl using a Höglof borer perpendicular to the stem and at breast height; B) Forest
1002 of *Pinus hartwegii* Lindl that grows on Ardillas dome; C) Detailed of the sample from a specimen
1003 of *Pinus hartwegii* Lindl. The ages range between 117 to 164 years.

1004

1005

1006

1007

1008

1009

Declaration of interests

The authors declare that they have no known competing financial interests or personal relationships that could have appeared to influence the work reported in this paper.

The authors declare the following financial interests/personal relationships which may be considered as potential competing interests:

Journal Pre-proof